MDPI

Article

Estimating Stream Bank and Bed Erosion and Deposition with Innovative and Traditional Methods

Paschalis Koutalakis [1] , **Georgios Gkiatas** [1] , **Michael Xinogalos** [2], **Valasia Iakovoglou** [1], **Iordanis Kasapidis** [1], **Georgios Pagonis** [1], **Anastasia Savvopoulou** [1], **Konstantinos Krikopoulos** [1], **Theodoros Klepousniotis** [1] **and George N. Zaimes** [1,*]

[1] Geomorphology, Edaphology and Riparian Areas Lab (GERi Lab), Department of Forestry and Natural Environment Science, International Hellenic University, University Campus, 1st km Dramas-Mikrohoriou, 66100 Drama, Greece; ptkouta@for.ihu.gr (P.K.); ggiatas@emt.ihu.gr (G.G.); valaiako@for.ihu.gr (V.I.); io_kasapidis@yahoo.gr (I.K.); gqpagon1995@hotmail.com (G.P.); anastasiaasavvopoulou@gmail.com (A.S.); blockerxd12@gmail.com (K.K.); kleptheodoros@gmail.com (T.K.)
[2] Astrolabe Engineering, Miaouli 26, 14671 Néa Erithraía, Attiki, Greece; mix@astrolabe.gr
[*] Correspondence: zaimesg@for.ihu.gr

Abstract: Understanding the contributions of stream bank and bed erosion will allow us to implement the most effective management practices. The objective of this study was to assess different methods to measure bank and bed erosion at different scales, specifically the watershed, reach and plot. Innovative and traditional methods were utilized. At the watershed scale, indices based on free satellite images were used. For the reach scale, indices were used, but the images with higher accuracy were purchased and captured by unmanned aerial vehicles (UAVs). At the plot scale, erosion pins, cross-sections and laser scanning were applied. The watershed scale analysis showcased "hot spots". These "hot spots" were reaches vulnerable to erosion and deposition. The indices of the purchased images were applied to these "hot spots" and allowed us to narrow the length of the reaches where UAV flights took place. These flight images located where erosion and deposition occurred. Finally, at the plot scale, laser scanning provided more detailed and accurate data at a greater scale compared to the traditional methods. The implementation of these methods allows us to find the areas vulnerable to erosion and deposition. These are the areas where nature-based solutions should be implemented to effectively mitigate erosion problems.

Keywords: watershed scale; reach scale; plot scale; satellite images; unmanned aerial vehicles; laser scanning

1. Introduction

Stream bank and bed erosion and deposition (Figure 1) are complex phenomena that can negatively affect societies and communities worldwide [1]. Fluvial erosion is the detachment of material from the stream/riverbed and its banks. Both erosion and deposition are natural processes, but anthropogenic activities and climate change have substantially accelerated their rates. Thus, stream bank and bed erosion and deposition monitoring and assessment are a priority worldwide because of the many negative impacts that they cause, but they can be difficult to achieve because of the episodic nature and the many factors that influence them [2]. These factors can be spatial, such as bank aspect, height and slope, or temporal, such as seasonal and yearly precipitation and streamflow events. Riparian land use also has a major influence. Typically, banks with natural vegetation have significantly less erosion than banks with agricultural activities [3].

Riparian areas are semi-aquatic ecosystems located in the transition area where the two adjacent ecosystems, the terrestrial and the aquatic, meet and integrate [4]. The aquatic system can be a river and stream and, along with the adjacent riparian area, can influence and impact of the fluvio-geomorphic processes including erosion and deposition.

Accelerated and extensive stream bank erosion and deposition can have detrimental effects on aquatic, terrestrial and semi-aquatic ecosystems [3]. Human alterations in land use and the developed infrastructure have increased the water concentration time of rainfall reaching streams. This is the result of the decreased water storage capacity of the landscape and increased surface runoff. Overall, the total amount of rainfall water reaching the channels has substantially increased, leading to higher annual and peak discharges. This leads to accelerated stream scouring potential and sediment transport capacity, leading to extensive channel incision [5,6]. A good understanding of stream bank erosion processes is necessary to manage streams, rivers and their riparian areas sustainably. Although many studies on stream bank and bed erosion have been conducted during recent decades, many facets of its processes are still not well explained because of their high temporal and spatial complexity [7–10].
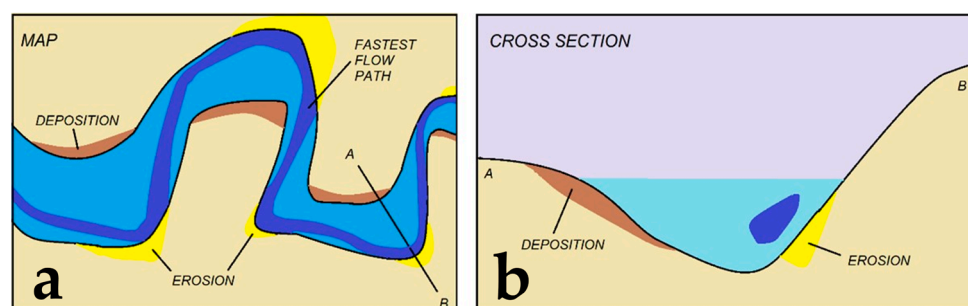

Figure 1. (**a**) Typical erosion (in yellow) and deposition (in brown) areas along a stream reach. (**b**) The cross-section A to B, from image (**a**), showing the erosion (in yellow) and deposition (in brown) areas. The dark blue indicates the area with the fastest stream flow.

Various methods and tools have been used to study and monitor stream bank erosion [11]. Traditional examples are the placement of erosion pins or Gerlach traps to monitor the geomorphologic changes by taking periodical field measurements [12]. Field monitoring stations, such as sensors of ultrasonic technology, can be used to estimate the distance changes between soil surface and the sensor [13]. In addition, photo-electronic erosion pins and the thermal consonance timing principle have been employed to increase the frequency and accuracy of erosion or deposition measurements [14]. Cross-section surveys and terrestrial laser scanners are other field methodologies that study soil erosion and deposition [15]. Field application erosion methods typically demand hard-working laborious tasks, are spatially limited and are time-consuming in contrast to remote sensing applications [16].

Remote sensing has been lately widely utilized for mapping, monitoring and predicting soil erosion [17]. An example of remote sensing monitoring is the utilization of satellite images [18] in combination with spatial datasets in geographical information systems (GIS) to implement the Universal Soil Loss Equation (USLE) model [19]. Other characteristic examples of models utilized for erosion include the following: (a) the Water Erosion Prediction Project (WEPP) model, which is a process-based continuous simulation model, (b) the Gavrilovic Equation [11], (c) the Soil and Water Assessment Tool (SWAT), which is based on the empirical Modified Universal Soil Loss Equation (MUSLE) [20], etc. Satellite images provide a wide range of possibilities for soil erosion monitoring in a fast way, especially in areas where a field survey is difficult or impossible due to the topography, dense vegetation or other local factors [21]. Vegetation and water indices based on satellite-derived images are very helpful for studies focused on soil erosion monitoring, since both the land cover and the soil moisture affect the soil erosion rate [22]. Lately, the combination of aerial photographs and images from unmanned aerial vehicles (UAVs) have been widely utilized in geomorphologic studies to monitor soil erosion or deposition areas [23]. UAV-based photogrammetry is considered the most advanced measurement approach in photogrammetry, resulting in high-accuracy and -resolution products captured by the remote-control

aircraft [24]. In addition, UAVs, apart from the usually attached camera, can carry other sensors for mapping, such as a light detection and ranging system (LiDAR) [25]. The flight can be manual, semi-automated or assisted and fully automated [26]. Higher spatial accuracy can be achieved either by using ground control points (GCPs) or by (global navigation satellite system) GNSS-tagged imagery [27]. GCPs are collected by using a rover and base station with a real-time kinematic (RTK) surveying system or by using a UAV with on-board an RTK positioning system [28]. Future monitoring belongs to UAVs since their increasing capabilities are enabling many new applications in photogrammetry. UAVs' performance has enhanced accuracy at larger scales and they are quicker compared to other methods [29].

Laser scanner instruments are based on the triangulation principle and are able to achieve high measuring accuracy (less than 1 mm) [30]. The laser scanner fits on a regular surveying tripod, while the survey data can be stored on its disk or a laptop. The scanned (X, Y and Z) data are stored on a local or global reference grid, while an expert software is used to process and develop the georeferenced point clouds or even orthomosaics [31]. There are several companies offering various 3D laser scanners to the market but their cost remains higher in contrast to other measuring techniques [32,33]. Terrestrial laser scanning (TLS) has proven to be an efficient and reliable method for collecting point clouds for a wide range of applications in architecture, engineering and construction [34]. Furthermore, TLS has been applied in earth sciences for many disciplines such as forest management, geology, seismology, natural hazards, geomorphology and glaciology, among others [35]. The use of TLS for measuring stream morphology is still in its early stages of research due to the complex environmental factor affecting the results (vegetation and other artifacts that are a considerable "noise") [36]. Heritage and Milan [37] successfully used TLS to measure the grain roughness heights of exposed bars and riverbed surfaces. Picco et al. [38] utilized TLS to study the short-term morphological dynamics and the processes of erosion and sediment deposition along a small gravel-bed braided river by comparing point clouds before and after a stream flow episode. Mayer et al. [39] compared three techniques for measuring stream bank erosion: erosion pins, total station and terrestrial laser scanning at nine site locations of the Indian Mill Creek watershed of Michigan, USA. They did not detect significant differences between measurement techniques but found a strong correlation between the last two techniques. Finally, TLS has been previously applied to collect high-resolution stream bank topography data and to estimate the volume of stream bank retreat [40].

This specific research presents the application of different methodologies to assess and estimate stream bank erosion and deposition at different spatial levels, from the watershed to the reach scale and finally to the plot scale. The many methods utilized and the technological advances require the assessment and comparison of the utility and ability to implement different methods for erosion and deposition. The study area was a typical Mediterranean watershed, the Aggitis watershed, in northern Greece. At the watershed scale, vegetation and water indices were developed based on freely available satellite imagery. At the reach scale, again, vegetation and water indices were utilized, but in this case, they were developed based on purchased satellite imagery of substantial higher resolution of targeted areas of the watershed. In addition, UAV-captured imagery was utilized to detect fluvio-geomorphologic changes in different cross-sections of selected reaches. The plot-scaled assessment included (a) the placement of erosion pins in selected stream banks with different land uses and soils, (b) taking cross-sections at the same locations and c) 3D laser scanning at specific vulnerable selected cross-sections. The ultimate goal of this research was to develop a framework of erosion and deposition measuring methods at different scales. The proposed framework will allow us to identify areas with the most geomorphologic activity (vulnerable areas of erosion and deposition). These areas should be targeted for erosion and deposition mitigation where nature-based solution implementation can help achieve the sustainable environmental management of the entire watershed.

2. Materials and Methods

2.1. The Study Area

The Aggitis River watershed is located in the Regional Unit of Eastern Macedonia in northern Greece (Figure 2). It belongs to the GR11 water division of Eastern Macedonia and the greater water basin GR11 of the Strymonas River. It covers an area of 2700 km^2 and it belongs to three regional units: (a) the Regional Unit of Serres (621 km^2 or 23%), (b) the Regional Unit of Drama (1647 km^2 or 61%) and (c) the Regional Unit of Kavala (432 km^2 or 16%) [41]. The watershed is surrounded by the mountain ranges of Menoikio to the west, Falakro to the north, the Lekani mountains to the east, Simvolo to the south and Paggaio to the southwest [42].
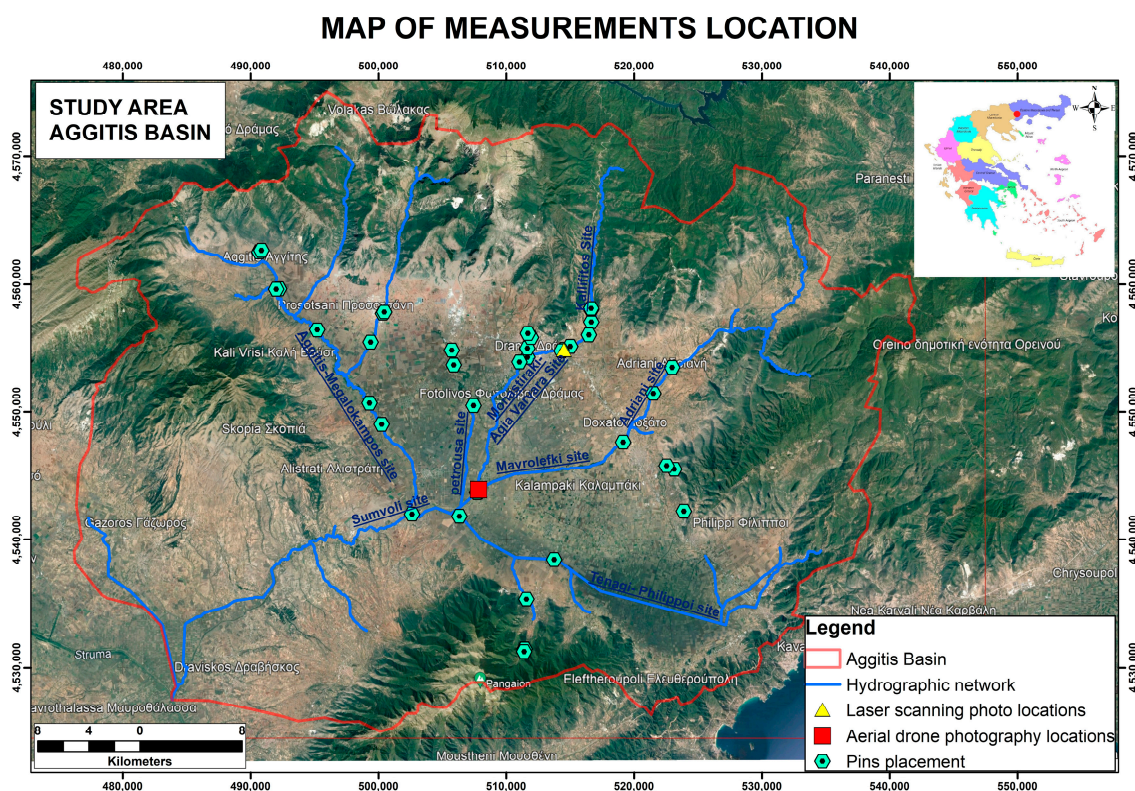

Figure 2. The Aggitis basin (red divide line) with the main stream network (blue lines) and the many monitoring locations with erosion plots and cross-sections of areas of different land use and soil types.

There are 21 different land uses that occupy the entire area. The four main land uses were selected to install erosion plots (forests/riparian zones, sclerophyllous vegetation, natural grassland/pastures and agricultural land) [43]. The watershed is characterized by the typical Mediterranean climatic conditions, land uses, soils, stream flows (ephemeral, intermittent and perennial), anthropogenic pressures and a channelized irrigation network for agricultural purposes [44]. In addition, several fluvio-geomorphological events have been recorded in the past. With limited studies on stream bank erosion and deposition in Greece and the Mediterranean, this study can be used as a benchmark for similar watersheds of the region. The Aggitis River length is 14.66 km and the water discharge volume is estimated as 495 m^3. The average annual precipitation varies from about 500 to 600 mm in lowlands, 600 to 1000 mm in the interior and exceeds 1000 mm in the highlands. The average annual relative humidity ranges from 65% to 70%. The average annual cloud cover is about 4.5 degrees, with the number of clear days ranging from 100 to 120.

The Aggitis basin is a tectonic depression created by faults in the wider area during the Alpine Orogeny. Based on the geologic map, of particular importance are the large

extent and thickness of the marbles located in the mountainous zone which have been affected by karst phenomena and tectonism (faults recorded in many places). Gneisses, schists and amphibolites are included within the marbles. The hilly and semi-mountainous areas are composed exclusively of tertiary sediments which, in their surface parts, consist of cohesive cobblestones and sandstones while at depths up to 250 m consist of marl. The lowland part consists of quaternary sediments, characterized by alternating layers of clay, gravel, sand and silt. In the deeper layers, clay materials and limestone silt prevail and are interrupted by lignite layers (depth reaches 370 m).

The marbles of the mountainous zone and the quaternary deposits of the plains are of great interest from a hydrogeological point of view. The marbles host huge amounts of groundwater. The underground water of these aquifers is discharged through a significant number of karst springs in the quaternary deposits. The aquifer of the Ochiro Basin is located in the mountainous zone north of the basin named as the Ochiro (Kato Nevrokopi) plateau and it is the source of the Aggitis River (Maara Cave or Aggitis Cave).

The peat area of Tenagi Filippon (55 km^2) with interspersed inorganic materials (mainly clay) of Holocene age is unique. This is a vulnerable hot spot as this area (formerly marsh and lake) is drained by a central agricultural ditch. Other hot spots are along the Aggitis River course and the mountainous torrents. Concerning the city of Drama, flooding was very frequent in the past, especially in the former torrent of the "19th of May". The area was urbanized and the specific torrent was covered by the street. The Kallifytos torrent is also an underground stream, but on the east side, entering the city, it has natural vegetation. It is considered dangerous, with many flooding phenomena along its course and with a large sediment transport capacity. Projects have recently been approved for its management with construction works. The below-mentioned are examples of flood events:

- Floods of 13–14 October 2002. Damage to 15.2 km^2 of crops in the plain of Drama.
- Floods of 18 November 2007. Great material damage in the local communities (Antifilippi, Eleftheroupolis, etc.)
- Floods of 10–11 February 2010. The fire service was called on dozens of occasions to clear water from flooded houses and warehouses.
- Floods of 10 March 2015. Major flooding phenomena in the Tenagi–Philippoi marsh plain, 80 square km of arable land under water.
- Floods of 13 December 2021. Flooding, landslides, infrastructure failures, road closures and transported materials (trees, rubble and other materials) in the Kallifytos torrent.

This study focused on the Aggitis watershed for the watershed-scaled assessment and afterwards examined specific reaches (e.g., Kallifytos torrents and Mavrolefki stream) and plots on selected stream banks and beds that had different land uses and soil types. Since stream bank erosion and deposition have high temporal variation [2], all monitoring methods were applied for at least one year to capture seasonal variability.

2.2. The Watershed-Scaled Assessment

2.2.1. The Free Satellite Images

Initially, free satellite images (Sentinel-2) were downloaded from the USGS EROS Archive (https://earthexplorer.usgs.gov last accessed on 12 February 2022). The Sentinel-2 satellite system has been developed and is being operated by the European Space Agency [45]. Sentinel-2 is an Earth observation mission from the Copernicus Programme that systematically acquires optical imagery at high spatial resolution (10 m to 60 m) over land and coastal areas [46]. The mission currently has a constellation of two satellites, Sentinel-2A and Sentinel-2B [47]. The images are multi-spectral with 13 bands in the visible, near-infrared, and short-wave infrared part of the spectrum [48]. Free satellite images covering different time periods (from winter to late autumn images) were downloaded to detect erosion-vulnerable areas. The images were acquired for dates when the vegetation cover was less developed, at the same enabling us to capture floods events (e.g., 18 February 2019). Another important parameter for the selection of the specific images was to have

less than 5% of cloud cover. Overall, a total of nine images were selected, three for each year of interest, 2019, 2020 and 2021. The specific dates of the images are as follows:

- 18 February 2019;
- 14 August 2019;
- 16 October 2019;
- 10 May 2020;
- 5 September 2020;
- 22 October 2020;
- 10 May 2021;
- 3 August 2021;
- 25 October 2021.

The selected images were processed in the ArcGIS software. The boundaries of the study area were delineated and used as a mask to crop the needed section of the satellite images. The next step was to produce the two indices: (a) the Normalized Difference Vegetation Index (NDVI) and (b) the Normalized Difference Water Index (NDWI). This was performed in the "Spatial Analysis Toolbox–Map Algebra–Raster Calculator" utilizing the corresponding spectral bands. The indices were classified into six groups/classes based on previous researchers' works (see Table 1) [49–51]:

Table 1. The classification of NDVI and NDWI values into the 6 classes.

No #	NDVI	Description	NDWI	Description
1	−1.0 to 0.0	No vegetation	−1.0 to −0.5	Very high drought or terrestrial vegetation
2	0.0 to 0.2	Unhealthy vegetation	−0.5 to −0.2	High drought or terrestrial vegetation
3	0.2 to 0.4	Poorly healthy vegetation	−0.2 to 0.0	Moderate drought
4	0.4 to 0.6	Moderately healthy vegetation	0.0 to 0.2	Poor water content/ low drought
5	0.6 to 0.8	Healthy vegetation	0.2 to 0.5	Moderate water content
6	0.8 to 1.0	Very healthy vegetation	0.5 to 1.0	High water content

2.2.2. The Vegetation Index

The Normalized Difference Vegetation Index (NDVI) is a frequently utilized proxy for vegetation cover in environmental and climatic change studies [52]. Equation (1) is used to calculate the NDVI as follows [53]:

$$NDVI = (NIR - Red)/(NIR + Red), \tag{1}$$

The NDVI is a dimensionless index that describes the difference between visible and near-infrared reflectance of vegetation cover [54]. The index receives values from −1 to +1. The higher the value (close to +1), the more it reflects high near-infrared (NIR) light, which means dense, greener and healthier vegetation cover, while clouds and snow are characterized by negative values. Typical vegetation values range from 0.2 to 1. Healthy plants, which are in very good condition, are reflected by values greater than 0.6 [55]. The values close to zero correspond to the absence of vegetation. The vegetation cover but also the road network and vehicles are clearly identified in the developed image, while the implementation of more enhanced calibration techniques could also separate the water surface. This index can be also used for soil erosion and drought monitoring [56,57].

2.2.3. The Water Index

The Normalized Difference Water Index (NDWI) is related to the water concentration levels on and in the soil or the existence of water bodies including flooded areas. Equation (2) is used to calculate it as follows:

$$NDWI = (Green - NIR)/(Green + NIR), \tag{2}$$

The NDWI was developed in 1996 [58] and is frequently utilized in remote sensing analysis of satellite images to map and detect surface water bodies. One of the key utilities of NDWI is the analysis before and post flood–storm events [59]. In addition, it can be used to predict erosion rates since it estimates the soil moisture [60]. Areas with higher values of the index indicate areas that may significantly influence the process of soil erosion and thus impact sediment concentration and deposition [61,62]. Similar to the NDVI, the values of the NDWI index vary from −1 to +1. Positive values (greater than 0.2) usually represent areas with high soil water concentrations, flooded areas or water bodies [63].

2.3. The Reach-Scaled Assessment

2.3.1. The Purchased Satellite Images

High-resolution satellite images were acquired in order to further assess the areas that were found to be vulnerable to soil erosion or deposition based on the results of the watershed-scale study (targeted areas). This enabled us to develop the vegetation indices at a different scale (reach scale) and study the areas in greater detail with substantially higher accuracy. The selected area of 25 km² in the Aggitis watershed was the confluence of the three main channels (Aggitis River, Tenagi Filippon Ditch and Agia Varvara Stream) in the Aggitis Dam in Symvoli Village, based on the watershed-scale analysis. A thorough study of the available satellite images, emphasizing the area after major events (dry/wet periods), was conducted in order to select those providing full coverage with no cloud cover. The final selection included 2 images captured by the Gaofen Satellite and 2 images captured by the WorldView-2 (WV2). The satellite images captured different extreme weather events (specifically after flood events). Gaofen is a series of Chinese high-resolution Earth imaging satellites launched as part of the China High-Resolution Earth Observation System (CHEOS) program [64]. The specific images have 80 cm resolution and were captured on 29 October 2016 and 21 March 2017. WorldView-2 is an imaging and environment-monitoring satellite from Maxar of the United States which was launched on 8 October 2009 that continues to remain operational [65]. The WV2 collects images that have a 50 cm resolution and the dates of the purchased images were 30 April 2019 and 11 June 2019. These images were used to develop the NDVI and NDWI for the selected areas based on the watershed analysis for the specific dates. The water boundaries of the natural channelized stream were delineated and any geomorphological changes (erosion/deposition along riverbanks and riverbed) were recorded in the ArcGIS 10.4 software.

2.3.2. The UAV-Based Orthomosaics from the UAV Flights

The UAV Flights

The flights were performed by using a powerful tetra-copter: the DJI Phantom 4 RTK. Using the DJI Phantom 4 RTK can be advantageous as it is user-friendly, low-cost (free and/or low-cost tools/software) and quick, as images can be captured in 10 min or less (depending on the area) and the results can be produced in a few hours (depending on the hardware capabilities). Their use also provides safety, since the user can hover the UAV remotely from a distance from the riverbanks and channel. The UAV is capable of capturing the stream bed and banks of a reach as its battery life is 30 min [66]. The UAV hovered at 50 m or 100 m height from the ground. The height was based on the conditions and dimensions of each stream reach that would allow us to capture the widths of its channel and its riparian zone in greater detail. The UAV can be coupled with the D-RTK 2 mobile high-precision GNSS receiver that supports all major global satellite navigation systems,

providing real-time differential corrections. This allows us to generate centimeter-level positioning data for improved relative accuracy. In addition, the GCPs included natural points (e.g., trees and rocks), human constructions and artificial marks (e.g., black/white targets in A4 size) that were used to calibrate the produced orthomosaics. The coordinates were taken by the GPS-GNSS Ruide Pulsar R6p device and the GPS-GNSS receiver of the UAV. The georeferencing was performed in the World Geodetic Reference System coordinate reference system (WGS84). The literature offers a wide range of choices for the number and spatial distribution of the GCPs used for photogrammetric applications [67].

The Photogrammetric Software

The Pix4Denterprize 4.5.6. is a powerful software capable of combining and merging the images based on common points; this methodology is commonly used for photogrammetric applications. Pix4D includes a set of tools, such as Pix4Dcapture, which is a mobile application that defines and executes the flight plan, and Pix4Dmapper that can be utilized to edit the captured data and create photogrammetric products [68]. The Pix4Dcapture tool is a mobile application that enables autonomous flight missions (grid, double-grid, polygon, circular, and free flight) and provides the estimated flight time, which is calculated based on the predefined mission parameters [69]. The Pix4Dmapper tool generates the point cloud, the mesh model, the texture, the orthomosaics, the 3D model (if images are captured from different ankles) and the digital surface model (DSM). One of the Pix4D's advantages is that it produces a feature report and a processing log which provides the detailed results [70]. Pix4D Mapper is a commercial software with the advantages that it is very easy to apply, even for beginners [71]. The developed orthomosaics and DSMs enable us to locate hot spots along the stream banks, even under water, either showcasing erosion or deposition areas.

2.4. The Plot-Scaled Assessment

2.4.1. The Stream Bank Erosion Pins

One of the best methods to capture the temporal (seasonally and yearly) and spatial (top and bottom bank) variability in stream bank erosion/deposition is erosion pins [72]. The main reason is because of the ability to frequently measure them and the high accuracy of the measurements. Erosion pins are narrow metal rods installed horizontally that are commonly used to measure the retreat or advancement of the streambanks over time [73]. They are suitable for a wide range of fluvial environments, inexpensive, and simple to maintain and measure. However, erosion pins can have difficulty accounting for larger scale (stream or reach scale) and very detailed spatial variability in streambanks. Totally, 400 erosion pins were placed in 40 selected positions throughout the stream network of Aggitis watershed (10 erosion pins per plot). The positions of the erosion plots were distributed equally among the four (4) main riparian land uses along the three main channels. The exact locations of the erosion pins were established by using the GPS-GNSS. Each plot had two spatially distinct erosion pin zones (five erosion pins in each one). The bottom zone was placed at 1/3 of the bank height (bottom bank) and the top zone at 2/3 of the bank height (top bank) (Figure 3). Vertical distances between the pins in the plots were 1 m. The erosion pins were 730 mm long, 7 mm in diameter, made of steel and inserted perpendicularly into the bank face.

Figure 3. Examples of stream bank erosion pins in Kallifytos torrent: (**a**) the two different height zones of erosion pin placements; (**b**) erosion pins marked with red paint for better identification; (**c**) placement of the erosion pins; (**d**) measuring erosion/deposition of the erosion pins.

Hooke [74] recommends that at least one-third of the pin remains buried in the stream bank face to reduce the risk of loss during a major erosion event. Pins also should not exceed 800 mm in length because when greater than that length, they can increase bank stability by reinforcing the soil, particularly increasing cantilever stability. The 7 mm diameter is small enough to cause minimum disturbance to the stream bank but large enough not to bend in high discharge events. The placement of erosion pins started on 13 November 2021 and finished on 5 December 2021. After the placement of the pins, five repeated measurements were made over a period of 2 years systematically and/or after major weather events (dry or wet days). The specific dates were as follows:

1.   25 April 2022;
2.   18 June 2022;
3.   8 October 2022;
4.   28 February 2023;
5.   15 June 2023.

2.4.2. The Stream Cross-Sections

Bench-marked cross-sections (Figure 4) were used to monitor the contemporary changes in the same plots where the erosion pins were placed [75]. The positions of the cross-sections were as follows: (a) one meter before the first pins, (b) in the middle of the erosion pin plot and (c) one meter after the last pins. The measurement days were

identical to the erosion pin measurement days mentioned above. The variables measured in each cross-section were as follows:

1. Length of each stream bank.
2. Length of the stream bed.
3. Slopes along each stream bank (left and right). More than one measurement was taken when slopes differed substantially along the bank.
4. Slopes along the stream bed. More than one measurement was taken when slopes differed substantially along the bank.
5. Cross-sections were compared among dates to detect changes in the morphological characteristics of the stream over time.
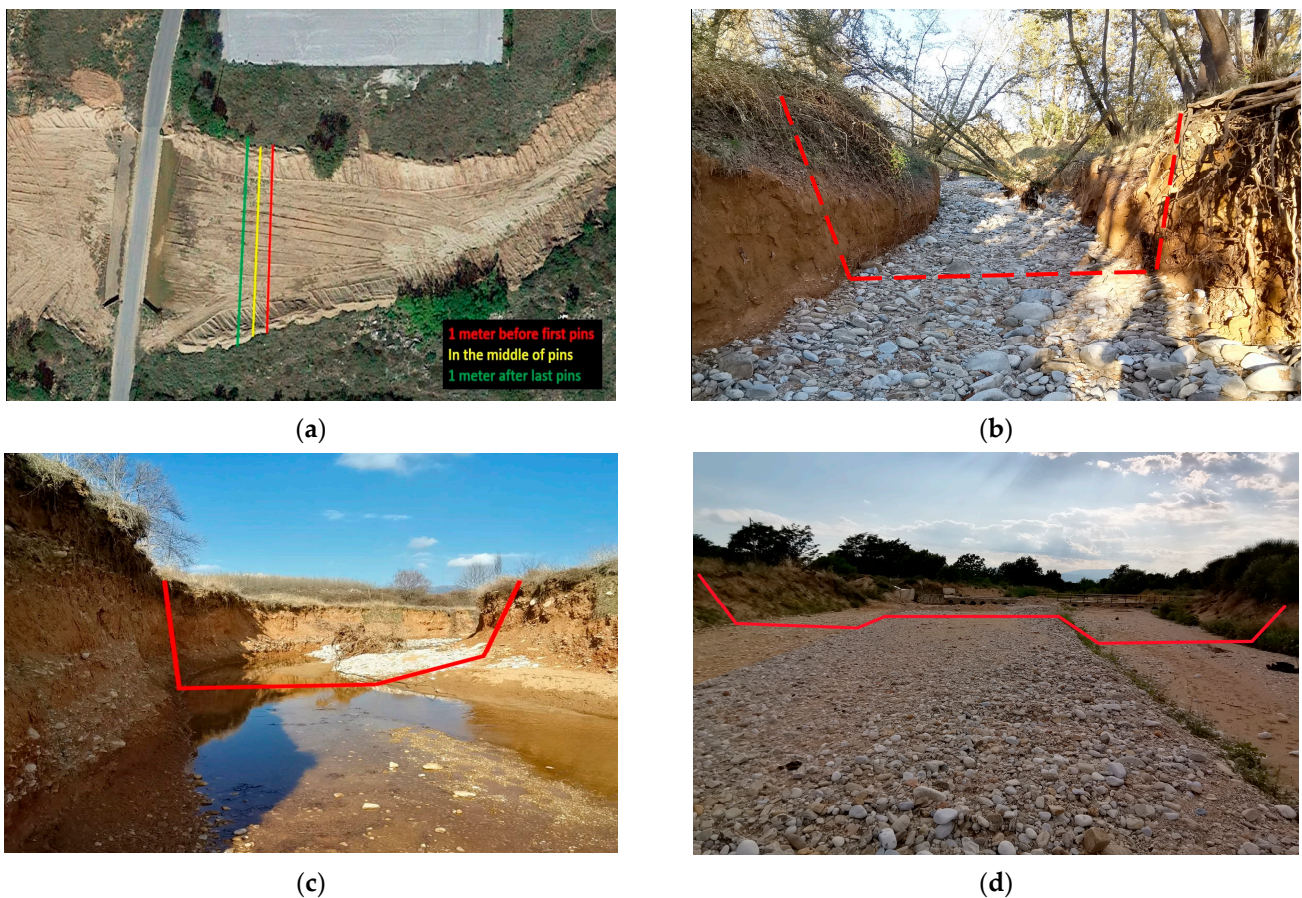

(**a**)

(**b**)

(**c**)

(**d**)

Figure 4. Examples of cross-sections in Kallifytos torrent: (**a**) UAV image captured an erosion cross-section; the different colors indicate the location of the three cross-sections; (**b**) field image of a narrow cross-section; (**c**) field image of a wide cross-section; (**d**) field image of a wide cross-section after torrential phenomena.

For the measurements of the above variables, the following equipment was used:

-   A GPS-GNSS receiver to find the locations of the plots;
-   A measuring tape for the channel's length (bank and bed);
-   An inclinometer for the slope of streambanks and streambed;
-   Height poles for the bank height/depth.

2.4.3. 3D Laser Scanning of Stream Cross-Sections

3D laser scanning is a method of collecting spatial measurement data from a distance. It is based on LIDAR (light detection and ranging) or laser radar technology: determining the position of an object by sending and receiving a laser beam [76]. The 3D laser scanners use a mirror mechanism that deflects the laser beam to scan the entire space or object with the desired density (resolution) and at a very high collection speed (recording up to

millions of points per second) [77]. With this method, a dense cloud of measuring points (3D point cloud) is quickly produced that documents with great completeness, precision and reliability the geometry of the space or the object captured [78]. 3D mapping was carried out on 18 February 2022 (1st date) and 24 April 2023 (2nd date) using the Faro Focus3D X 130 laser scanner in order to assess any geomorphological changes on the stream banks and bed of three different sites of interest. Only the Kallifytos site (X: 41.146953, Y: 24.171873) data are presented as the most representative channel type of the study area (see Figure 5).
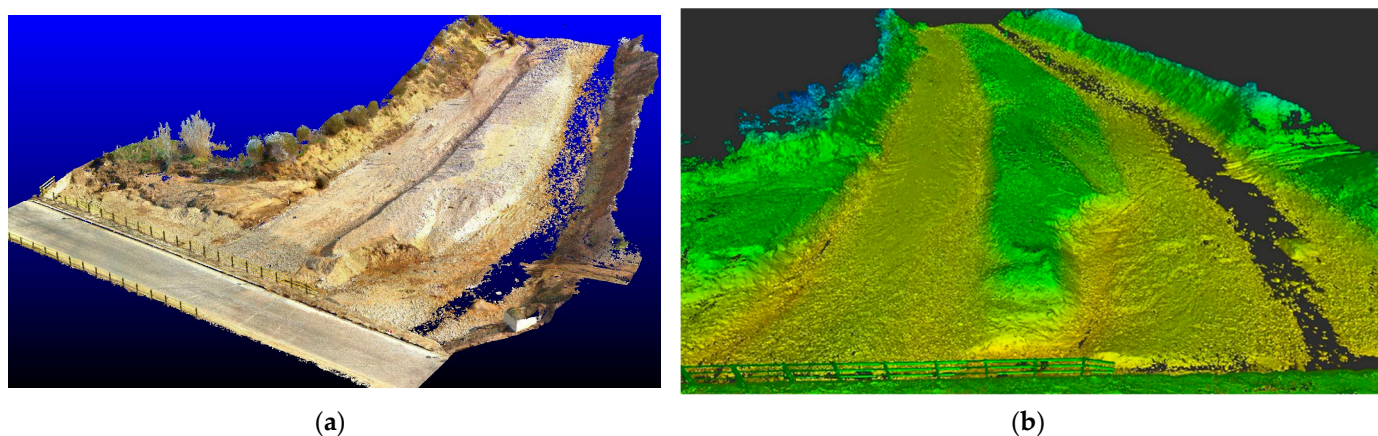

(**a**)   (**b**)

Figure 5. An example of 3D scanning capturing (**a**) the RGB image and (**b**) the 3D point cloud from the Kallifytos torrent.

3D scanning was conducted from an appropriate number of scanning positions to completely cover the area of the channel to be mapped, with an average resolution of 1 cm. Alongside the scan, high-resolution panoramic images were taken from each location via the scanner's built-in camera. Eighteen (18) scan sites were used on the 1st date, while 17 sites were used on the 2nd one.

To process and analyze the captured data, the Faro Scene, Autodesk ReCap 2023.1.1 and Gexcel Reconstructor 4.4.1 software were utilized for the following:

- Processing of the georeferenced measurements (control points).
- Generating the point cloud for each scan position.
- Preprocessing of the point clouds (cleaning, filtering, quality control, target identification, etc.).
- Aligning the clouds from successive scan positions. This was performed with the cloud-to-cloud methodology using the least squares and iterative closest point (ICP) algorithms.
- Georeferencing based on georeferencing measurements.
- RGB color rendering from panoramic images.
- Creating a single-colored 3D georeferenced point cloud.

The produced deliverables were color 3D point clouds for the Kallifyto site per date and various visual 2D and 3D visualizations (in the form of digital images) of the 3D point clouds. This enabled us to visualize the stream bank and bed of the captured areas and to understand and interpret the geometric changes in their slopes between the two measurement dates.

3. Results

3.1. The Watershed-Scaled Assessment

3.1.1. The NDVI

The distribution of the NDVI classes differed for each satellite image (Figure 6). The NDVI for class #6 was present only during spring and summer, specifically on 14 August 2019, 10 May 2020, 5 September 2020, 10 May 2021 and 3 August 2021, with a maximum

coverage of 8%. The NDVI for class #1 was only visible on the 08.02.2019 satellite image (4%), with classes #2 and #3 dominating with a coverage of 38% and 42%, respectively. In the autumn months, specifically, 16 October 2019, 22 October 2020 and 25 October 2021, the NDVI classes #3 and #4 (both approximately 33%) had the highest percentage followed also by classes #2 and #5. On all of the other satellite images, the NDVI class #5 had the highest coverage percentage and was dominant.
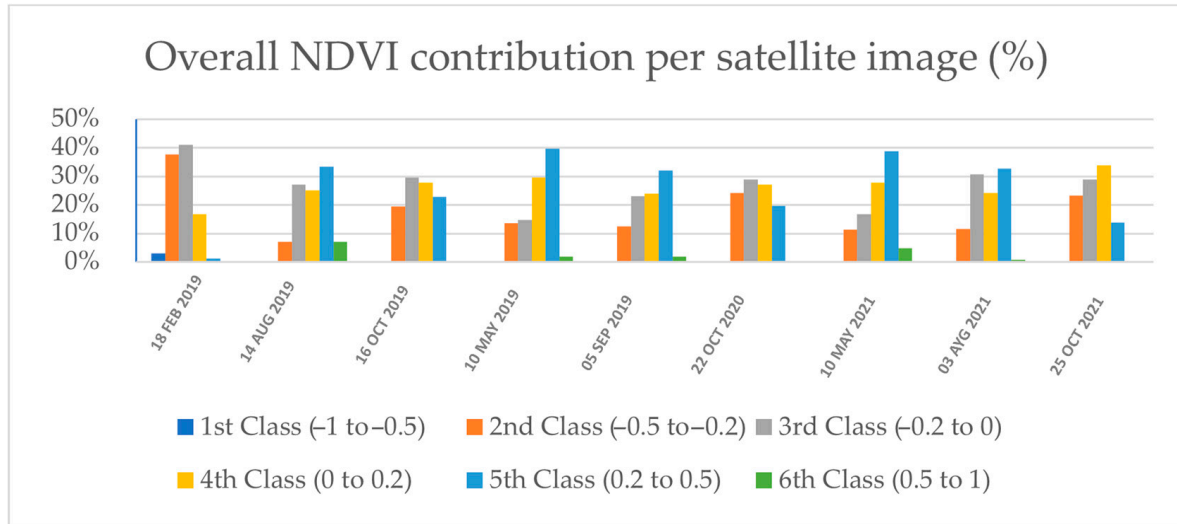

Figure 6. The percentages of the NDVI six classes for each satellite image.

3.1.2. The NDWI

The NDWI class #2 was dominant in all satellite images, with percentages ranging from 50% to 72%, followed by the NDWI class #1 (19–45%) (Figure 7). The specific classes correspond either to terrestrial vegetation (mostly sparse sclerophyllous vegetation and pastures) but also to bare soil, which indicates a high degree of soil erosion mostly on higher altitude and intense slopes of the surrounded mountainous areas. The classes #5 and #6 were very limited and adjacent to existing water resources that enabled us to narrow this study focus to the "hot spots" of soil erosion: areas near floodplains of torrents/streams/rivers.
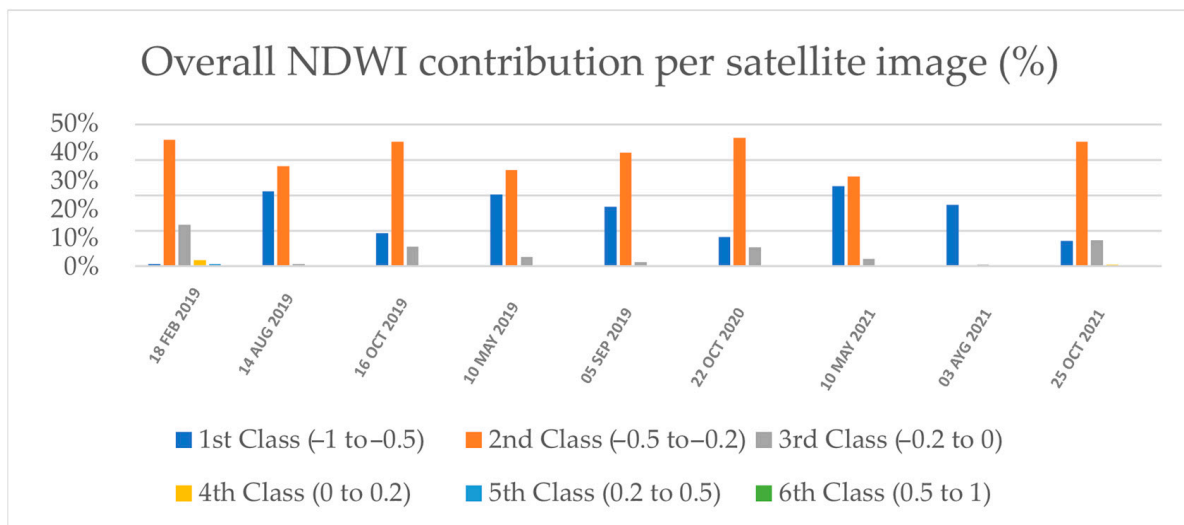

Figure 7. The percentages of the NDWI six classes for each satellite image.

3.1.3. Soil, Land Uses and Slope Characteristics

Three characteristics, soil types, land uses and slopes percentages, were calculated based on the developed NDVI and NDWI maps (for each satellite image). Specifically, the percentage of the indices' classes for these characteristics could highlight which reaches would be more vulnerable to erosion or deposition (higher percentages of a certain class).

The NDWI class #6 was dominated by "Calcaric Fluvisols", "Calcaric Leptosols" and "Dystric Leptosols". This class represents flat areas with vulnerable soils to erosion and deposition affected by the stream network in the pilot area of the Aggitis River watershed. Furthermore, if we include the NDWI class #5, the areas were dominated by "Calcaric Fluvisols", "Eutric Histosols" and "Vertic Cambisols". On the other hand, the "Dystric Cambisol" was the soil that dominated the areas of the NDWI class #1. Concerning the NDVI, classes #1 and #2 (which may indicate soil erosion) had the highest percentages for "Vertic Cambisols", "Calcaric Fluvisols", "Chromic Luvisols", "Calcaric Leptosols" and "Eutric Histosols" soils, although this was highly different in each satellite image. There were occasions when class #6 of the NDVI was not recorded at all.

The urban areas (specifically industrial or commercial units), non-irrigated arable land and complex cultivation patterns have the highest share in land cover for the NDVI class #1. Furthermore, the land uses, permanently irrigated land, natural grasslands, sparsely vegetated areas and water courses, also had a significant contribution. It must be highlighted that similar land uses were recorded for potential erosion and deposition in the NDWI. Specifically, complex cultivation patterns and industrial or commercial units had high NDWI #6 percentages, followed by water courses, permanently irrigated land and non-irrigated arable land but also broad-leaved forests that had high NDWI #5 percentages.

The slope (%) had five discrete categories based on the natural breaks of its values: (i) areas with slope angles less than 12% (gentle slopes), (ii) areas with slope angles between 12% and 29%, (iii) areas with slope angles between 29% and 48%, (iv) areas with slope angles between 48% and 72%, and (v) areas with slope angles greater than 72% (steep slopes). Gentle slopes stood out for their extent and moderate exposure to erosion, especially based on the NDWI (classes #1 and #2). In contrast, steep slopes dominated areas characterized by no or sparse vegetation which form stream network valleys.

3.2. The Reach-Scaled Assessment Results

3.2.1. The Purchased Satellite Images

An automatic classification of the indices' values in ArcGIS enabled us to delineate the boundaries of the water surface. The area captured by the purchased satellite images was the main water course near the confluence of the Aggitis River in the plain of the Regional Unit of Drama. According to the watershed-scale analysis, this area along these perennial streams is one of the most vulnerable to soil erosion and deposition. Many changes have been recorded throughout time on the stream banks and the main channel geomorphology (especially in the confluences where the tributaries meet). Figure 8 includes the boundaries as polylines in four different locations for different dates.

3.2.2. The UAV Images

Based on the previously purchased satellite image analysis, the Mavrolefki reach of the hydrologic network of the study area is one of the most vulnerable. This reach collects the water from Drama city but also from Kalabaki and Doxato towns. This reach is located along the southeast side of the village Mavrolefki (Y: 41.053137, X: 24.104371 in WGS84) where there was a temporary earth-filled dam (or embankment dam) established during the summer to store water from agricultural purposes (Figure 9). During the UAV flight (23 October 2021), this dam was destroyed, and the flowing water even covered the nearby gravel road for agricultural vehicles. The Mavrolefki reach (part of Tenaghi stream) has intense meanders that are covered with water during high rainfall events. The entire stream has many "hot spots" of erosion and deposition, including islands in the main channel bed (Figure 9). In addition, there were other locations along the same reach with litter present

(plastic bottles, tree trunks or tires) as well as locations where the color of the water was cloudy, probably due to agricultural practices (see Figure 10).
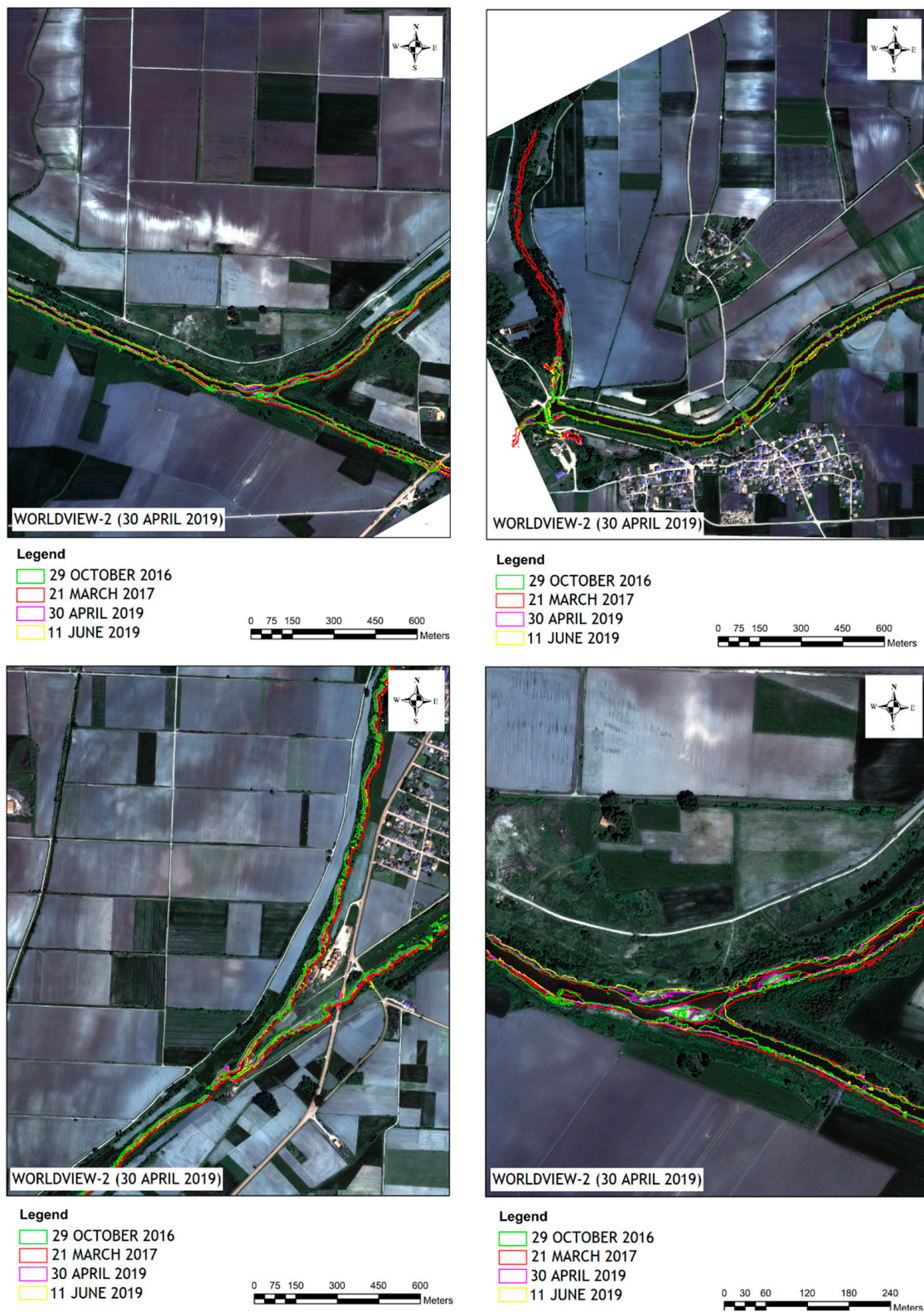

Figure 8. The stream water boundaries are seen as polylines in four different locations on four different satellite dates. The background satellite image is the same for all dates.
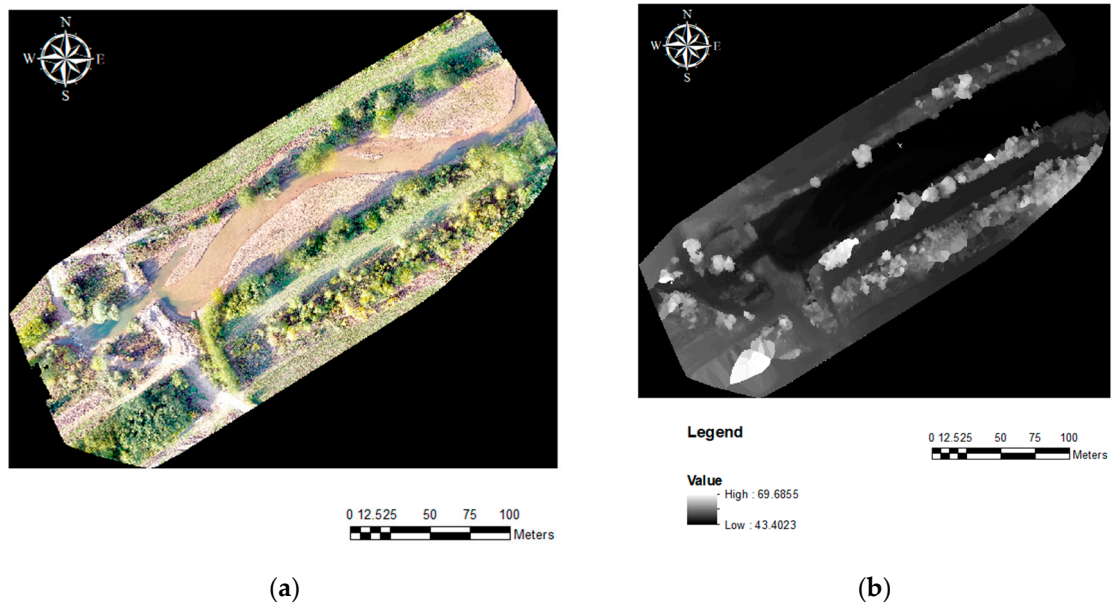
(**a**)   (**b**)

Figure 9. (**a**) The orthomosaic and (**b**) the DSM for the Mavrolefki reach near the Mavrolefki village.

(**a**)   (**b**)

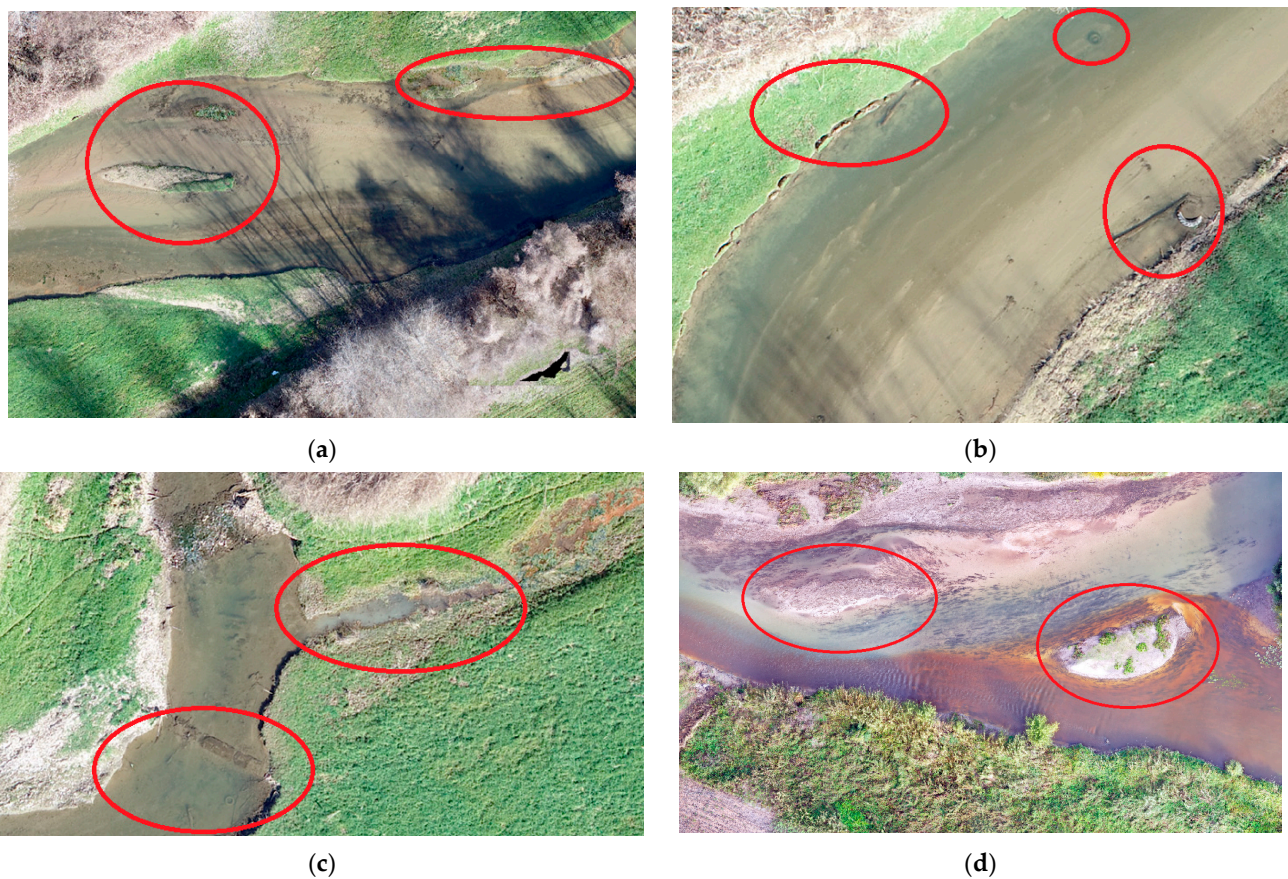(**c**)   (**d**)

Figure 10. Examples (in red circles) of soil erosion, deposition and littering in different sections of the Mavrolefki reach detected by using UAV images: (**a**) sediment deposits as small islands and stream bank erosion, (**b**) stream bank erosion and plastic tires in the stream, (**c**) littering accumulation and cloudy water and (**d**) sediment deposits as small islands in the confluence of two streams. Different color due to a rainfall event that occurred mainly in one of these two watersheds. Water color is much clearer in the top than in the bottom.

The second targeted location of the same reach (Figure 10a,b) is at the main road network (Y: 41.047003, X: 24.094152 in WGS84), specifically at a bridge. The specific stream reach has also intense meanders that are covered with water during high rainfall events. The DSM was very helpful to distinguish the main channel curves of current water flow. There are parts of the stream banks that were vulnerable to soil erosion and others that are characterized by soil deposition. Another important point that needs to be mentioned is that the land use of the adjusted area is grazed pastures which enhances soil erosion.

Another location of the same stream is at its confluence with other streams (Y: 41.045076, X: 24.090637 in WGS84) that is mainly characterized by frequent sediment deposition (Figure 10c,d). The specific reach reveals both soil erosion (on the north side) but also sediment deposition (on the south side) and small island formation at the junction of the two stream networks. The UAV flight was performed during a rainfall event that covered the east side of the watershed of Aggitis and supplied with water the area of Tenagi Philippon (Kavala region) in contrast to the Drama region which was not affected by the rainfall event and its stream was not supplied with water. This fact led to a color difference due to the high sediment concentration in the streams from Kavala.

3.3. The Plot-Scaled Assessment Results

3.3.1. The Stream Bank Erosion Pins

The monitored banks (Figure 11) show differences according to the land-use types. The positive values indicate erosion, while negative values refer to deposition. In natural grazed grasslands, there are fluctuations in the erosion of the banks after intense rainfall events. These differences in erosion and deposition appear more on the pins at 2/3 of the bank height (Figure 11a,b). In the riparian forested areas (Figure 11c,d), the erosion of the bank is very low and in most of the measured pins does not exceed 10 cm. Overall, we can state that the observed changes were not substantial. In the agricultural areas, there was extreme erosion measured, in some cases exceeding 40 cm on the monitored banks (Figure 11e,f). It is important to mention that in several cases, erosion pins were completely lost. This happened on the first (25 April 2022), second (18 June 2022) and fifth measurement (15 June 2023). Also, for this land use, we observed that at 1/3 of the bank height, there was more erosion than at 2/3 of the bank height. At locations characterized by sclerophyllous vegetation, there were also strong geomorphologic changes, with both erosion and deposition recorded (Figure 11g,h). Specifically, the erosion rate was lower at 1/3 of the height, approximately 5 cm, than at 2/3 of the bank height, ranging from 10 to 15 cm.

3.3.2. The Stream Cross-Sections (Plot Scale)

Erosion and deposition events were recorded on the sampled surfaces with the changes in the dimensions of the cross-sections (Figure 12). In general, the changes were small, but several large differences were observed between the measurements that reached 1–2 m. Such differences were recorded more in agricultural areas, while for the other land uses such as grazed natural grassland and sclerophyllous vegetation, the changes in the cross-sections were smaller, with a difference ranging from 0.30 to 0.80 m. Finally, it is important to mention that in riparian forested areas, the changes in the cross-sections were minimal, with values ranging from 0.10 to 0.20 m. An example is the Kallifytos torrent, where the material which was transported and deposited was mainly located in the area upstream of the Irish Bridge (before the east entrance to the city of Drama). The material deposited is frequently removed by the local authorities using heavy bulldozers that can compact the stream bed material (Figure 12a).

(**a**)

(**b**)

(**c**)

(**d**)

(**e**)

(**f**)

(**g**)

(**h**)

Figure 11. Bar diagrams of erosion and deposition for the four land uses (positive values = erosion and negative values = deposition). (**a**) Erosion and deposition rates at 1/3 of stream bank height in natural grazed grasslands, (**b**) erosion and deposition rates at 2/3 of stream bank height in natural grazed grasslands, (**c**) erosion and deposition rates at 1/3 of stream bank height in riparian forested areas, (**d**) erosion and deposition rates at 2/3 of stream bank height in riparian forested areas, (**e**) erosion and deposition rates at 1/3 of stream bank height in agricultural areas, (**f**) erosion and deposition rates at 2/3 of stream bank height in agricultural areas, (**g**) erosion and deposition rates at 1/3 of stream bank height with sclerophyllous vegetation and (**h**) erosion and deposition rates at 2/3 of stream bank height with sclerophyllous vegetation.
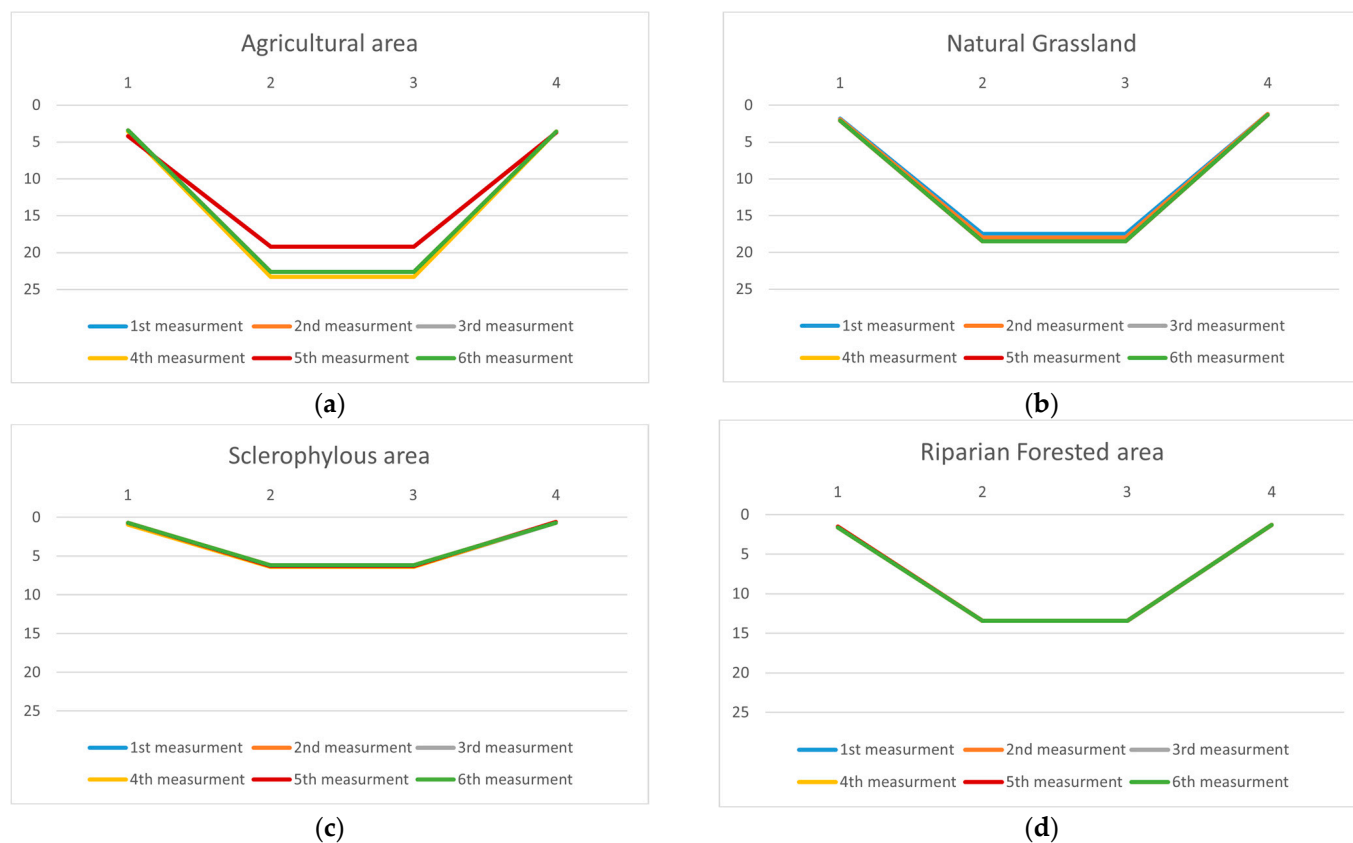
Figure 12. A typical cross-section of each land use in six different areas: (**a**) agricultural area; (**b**) natural grasslands; (**c**) sclerophyllous vegetation; (**d**) riparian forests.

3.3.3. The 3D Laser Scanning Streams' Cross-Sections (Plot Scale)

The Kallifytos torrent is a typical intermittent Greek torrent that has flash flood risk potential particularly after heavy rainfalls [75]. The torrent was selected (erosion pins, cross-sections and laser scanning) because it has a diverse fluvio-geomorphologic profile, with rapid changes in the channel and bed shape due to the large amounts of water, sediments and debris transported [79]. The Kallifytos torrent passes through chutes under the city of Drama before discharging into the Agia Barbara stream, which is a tributary of the Aggitis River.

The comparative 3D sections from the Kallifytos reach based on the 3D field scanning allowed us to estimate the fluvio-geomorphological changes between the two surveying dates (Figure 13). The point clouds (Figure 13a: first survey and Figure 13c: second survey) along with the mesh models (Figure 13b: first survey and Figure 13d: second survey) were developed. Furthermore, five selected cross-sections were drawn to estimate the material loss or gained between the two survey dates.
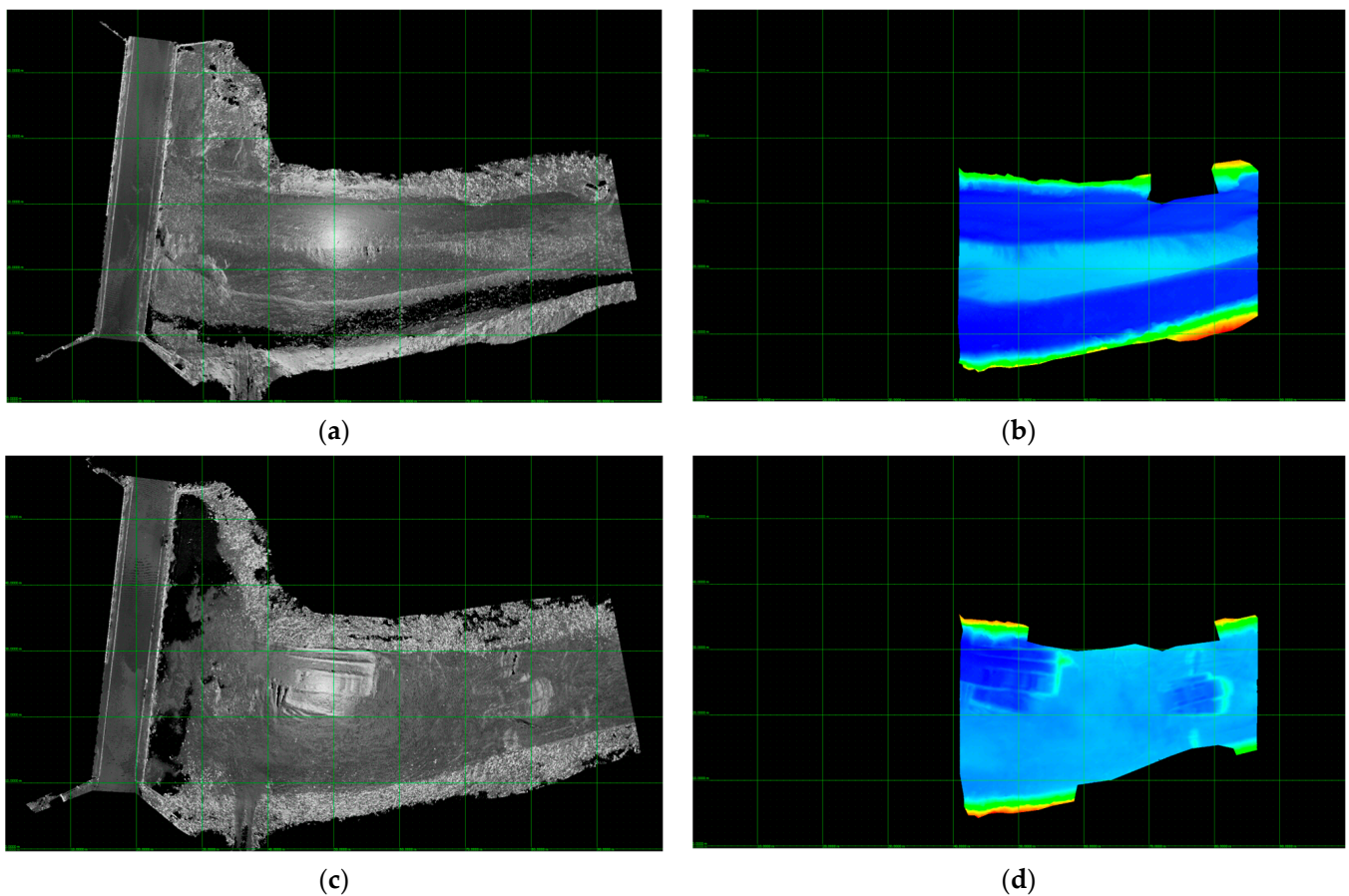
Figure 13. The 3D outputs based on the 3D laser scanning application in Kallifytos torrent reach: (**a**) the point cloud (1st survey); (**b**) the mesh model (1st survey); (**c**) the point cloud (2nd survey); (**d**) the mesh model (2nd survey).

There are clearly visible geomorphological changes in the stream bed. During the first survey, there was deposited material in the center of the stream bed which was distinguished by the lighter blue color. The second survey captured the manmade sand excavations and the removal of deposited material carried out by municipality bulldozers (rectangular formations depicted in darker blue color). There were also differences in the stream banks which are depicted more clearly in the selected 2D cross-sections of the same captured location (Figure 14). In the cross-sections, the first survey is shown in red and the second in green, while both the X and Y axis scales are in meters. Specifically, height differences ranging from 0.00 to 1.26 m of removed material (section B) were detected. The removed material was estimated to be equal to 412.01 m^3 for the stream bed, 2.55 m^3 for the north stream bank and 2.21 m^3 for the south stream bank (Figure 14). Similarly, the gained material was estimated to be equal to 2.82 m^3 for the stream bed, 0.58 m^3 for the north stream bank and 0.70 m^3 for the south stream bank (Figure 13).
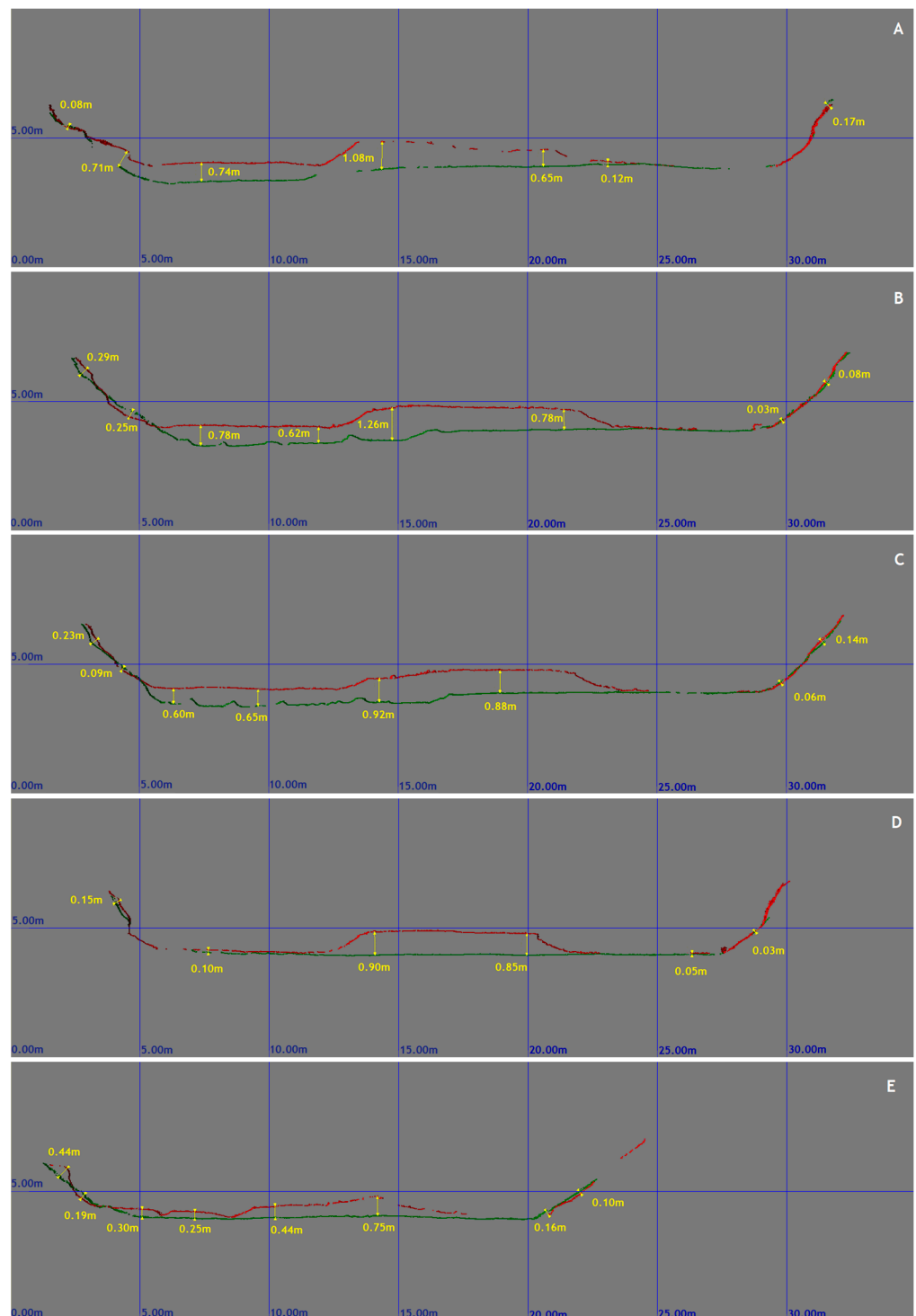
Figure 14. The selected five 2D cross-sections based on 3D laser scanning application in Kallifytos torrent reach. The red lines indicate the 1st survey and the green lines indicate the 2nd survey.

4. Discussion

Erosion and deposition are two of the main fluvio-geomorphologic processes that at both the watershed and/or stream channel scale need to be measured and understood in order to achieve sustainable watershed management, especially under the auspices of the Water Framework Directive and the EU Green Deal. In this study, different measuring methods were utilized at the watershed, reach and plot scale to assess erosion and deposi-

tion (Figure 15). These methods included remote sensing, UAV monitoring, terrestrial 3D scanning and traditional commonly used field monitoring tools (pins and cross-sections).
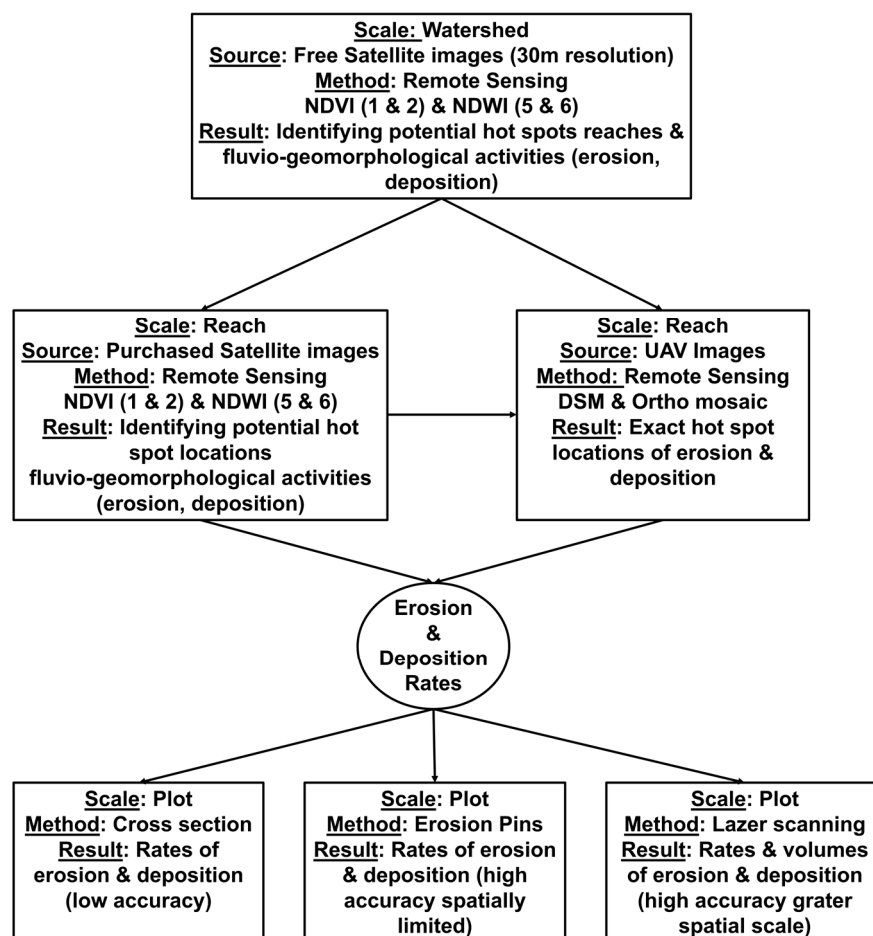

Figure 15. The flowchart of different stream bank and bed erosion and deposition methods. The methods are for different scales: some are for identifying erosion and deposition hot spots and others are for measuring exact rates.

The technological and methodological advancements in the field of Earth observation has contributed to the widespread increase in the use of satellite remote sensing approaches that have enhanced the monitoring of the Earth's surface and its changes [80,81]. Today, there is a readily available large collection of imagery in Google Earth, including satellite, aerial, and even 3D and street view images. Furthermore, free available satellite imagery (e.g., Landsat and Copernicus) is of high importance for remote sensing in geomorphology [82,83]. Free SENTINEL-2 satellite images have been used in various studies to develop indices, as they are competent at highlighting differences in vegetation and water content. The NDVI enables the monitoring of ecosystem and fluvio-geomorphological changes based on the large-scale land monitoring/mapping of floodplains [84]. In addition, as a globally used index of vegetation's health and moisture presence, it is used for the assessment of watershed soil erosion and sediment yield in the floodplains [85]. The NDWI, the other index utilized, can characterize soil and vegetation moisture content before and after flooding events. In addition, it is used to monitor the channel migration [86]. Channel bank and bed erosion occurs mainly in the floodplains; thus, the NDWI was used to detect the water presence lines that can lead to short-term stream bank erosion [87,88]. Its effectiveness decreases with intermittent or ephemeral streams typical in Mediterranean ecosystems [89]. Both indices enabled us to map the most vulnerable areas to erosion and deposition along the stream network and their floodplains. The results of the NDVI and

NDWI showcased the most critical areas prone to erosion. Those which belong to NDVI #1 and NDVI 2 classes represented 7–40%. On the other hand, the affected areas by water (areas adjusted to the water courses and floodplains, NDWI classes #5 and #6) represented only up to 1% of the total studied area. It must be noted that these areas are highly important for the dynamic procedures of stream bank erosion and sediment transportation and should be focal points for stream conservation [12]. In general, erosion occurs when the force of the river's flow removes sediment from the stream bed and banks, widening and deepening the river channels. It is typically caused by the high velocity and turbulent flow of water [90]. The confluence of rivers are such dynamic locations of a hydrologic network where soil erosion or deposition have high rates [91]. The convergence of flow often leads to erosion (downcutting) of the stream bed. Tributaries also alter the hydraulic geometry of the receiving streams (due to stream water turbulence) including width, depth, and bar size and occurrence. Typically, they can alter the particle size distribution, either coarsening or fining the channel bed material. The morphological effects of confluences tend to be most pronounced in lower-gradient portions of rivers. These areas are "hot spots" and allow us to determine potential targeted areas so we can move management from the watershed to the reach scale. Additionally, we used ancillary information (soils, land cover and slope) to determine whether we can find any connection between these characteristics and vulnerability to erosion and deposition (watershed-scale approach).

These vulnerable reaches were further investigated by the comparisons of purchased satellite images that had substantially better resolution. These images were taken before and after flood events in order to capture deposition and erosion phenomena. Low spatial resolutions images are appropriate to be applied at perennial and large dimension temporary streams and for the identification of individual large and medium-sized gullies but do not allow for gully growth analysis with sequential imagery that requires higher resolution [92,93]. Medium and low-resolution images are effective for erosion risk mapping if they present data shortly before and after the first erosion event [94]. High-resolution satellites have enhanced the ability to detect and monitor individual small-scale geomorphologic features [95]. Studies have applied high-resolution products for monitoring erosion by mapping ephemeral streams, as well as smaller (even temporary) gullies and rills that are not covered by dense vegetation (dry and semi-dry environments) [96–99]. There is a place to utilize both free and commercial satellite products, as nowadays there are more options for economical topographical mapping [100]. The selection of higher to low spatial resolution satellite products depends on the ground sampling distance needed based on the research objective [101]. In addition, the size of the study area and the available funds must be considered. High-resolution imagery should be used for study areas of 20–100 km^2 study, while low resolution for areas > 100 km^2 [102]. This is the reason we proposed to firstly use the free low-resolution satellite imagery in the watershed-scale phase (in our case study Aggitis basin is 2700 km^2) and secondly, to use higher-resolution products (if available) on the selected "hot spots". The results of this study show the utility of both and how they can be complimentary to each other. The free satellite images can indicate where there is a need (hot spots) to purchase the high-resolution satellite images. This allows for the cost-effective use of funds, and the more targeted approaches for the placements of conservation practices (e.g., nature-based solutions) can be implemented with higher-resolution purchased images.

Furthermore, UAV-based orthomosaics were developed in some of these vulnerable selected reaches. UAVs have been applied worldwide as a monitoring methodology to improve the monitoring of fluvio-geomorphologic changes [103,104]. The advantages of UAV-based photogrammetry are the ability to reconstruct the stream bank topography in very high detail and very quickly [105]. The results produced by the UAV's flights enabled us to monitor the fluvio-geomorphologic changes again at the reach scale but also at a smaller scale and with enhanced resolution. Orthomosaics developed by UAV images taken at different times provide detailed stream channel features to detect changes between periods [75].

Site assessments and in-situ measurements (erosion pins, stream cross-sections and 3D laser scanning) have been used to evaluate and monitor the stream bank erosion or deposition at the plot scale. The analysis of the results from the field measurements of this study showcased high erosion on some stream banks, especially after extreme rainfall phenomena. In several plots, bank erosion exceeded the 50 cm, while in a few, deposition was also recorded. Deposition was recorded mainly in sclerophyllous vegetation (both bank heights) but also in agricultural areas (1/3 of bank height). Stream bank erosion was high in most of the natural grasslands/pastures and agricultural areas. Agricultural and livestock activities are highly associated with erosion phenomena since they weaken bank stability though different activities [106]. Finally, it should be noted that on stream banks covered with riparian vegetation, the erosion was limited or non-existent. Many studies have shown that maintaining or re-establishing the riparian vegetation is optimal to reduce erosion and a highly recommended nature-based solution [107]. Land cover types, and their changes, have different hydrological and geomorphological effects on controlling bank stability or enhancing soil erosion [108]. Forests are considered to stabilize slopes and banks, while human intervention on stream banks and riparian zones may reduce stability [109,110]. For agricultural lands, the implementation of conservation practices can have a significant impact on soil erosion reduction, especially in the Mediterranean dry region which suffers from tillage agriculture erosion impacts [111]. The produced point clouds of the plot-scaled laser scanning approach were of high resolution and estimated soil volume changes (erosion or deposition) before and after events. Specifically, soil deposition was recorded after an extreme flood event, while soil removal (erosion) was detected after excavations were performed by bulldozers. The amount of stream bed and bank material was also easily estimated in these specific cross-sections through the point-cloud comparison when riparian or stream bed vegetation was limited or absent [112]. Overall, the results of laser scanning and traditional field plot measurements were similar. The advantage of laser scanning was the higher accuracy and also the larger scale it can implemented on in comparison with traditional methods.

The studied targeted reaches of Mavrolefki stream showed that erosion can lead to the formation of sandbars and islands within the stream channels. Deposition occurs when sediment carried by the stream flow decreases, and thus settles and accumulates in the bed. This is also evident in the main course of theAggitis River and its tributary streams with intermittent flow. On the other hand, Kallifytos showed more episodic flow characteristics, typical of Euro-Mediterranean torrents (ephemeral and intermittent flows) [113]. For most of the year, these torrents have no flow, but a few times during the year, they can have very high flows and transport large amounts of sediment.

The results of this study are similar to others that utilized such methodologies, although our study was the first detailed research incorporating all of these methods [23]. UAV-based surveys have been also conducted by the authors before, in selected reaches of the region, for the first time with successful results [75]. Flooding is a common phenomenon in the Aggitis basin after extreme rainfall events or snowmelt causing serious damage in the area [114]. There is high connectivity between extreme flood events and stream bank and bed erosion and deposition in the channels and floodplains [115]. Anthropogenic activities and climate change are accelerating soil erosion, fluvial activity and extreme flood events [116]. Along the Aggitis River and its tributaries, alluvial aggradation was accelerated by 6000 BP due to climate change between 6500 and 5000 BP [117]. Such events were also recorded during the Ottoman period, linked to the intensification of farming in the Aggitis river plain along with the increase in grazing and logging in the surrounding mountainous areas [118]. This study also revealed that extensive erosion occurs by anthropogenic activities in channels when the major land cover in the riparian areas and the watershed is agricultural or grazed grasslands.

The different studied stream bank and bed monitoring techniques presented advantages and disadvantages that have been presented previously. Their selection and application is highly dependent on the scale and accuracy required, the site-specific conditions and

the experience of the researcher. Traditional field monitoring approaches can be laborious, time-consuming and resource-demanding, especially when examining lengthy reaches of rivers or streams [119]. Erosion pins can be used in vegetated banks but with coarse spatial and temporal resolution. UAV mapping or laser scanning have higher resolution for larger reaches but can have problems when the stream banks have dense vegetation. A UAV survey requires low vegetation, as tree canopy may cover the ground, while terrestrial laser scanning can be applied in a forested environment when employing the vegetation filter to extract the tree trunks, but it is difficult, or even impossible, when riparian vegetation is low or mixed. As a consequence, the final choice of the appropriate technique depends on the goals of the project and the desired resolution, the stream bank or bed conditions, and the available resources, tools and finances [39].

5. Conclusions

Stream bank and bed erosion and deposition are natural process, but anthropogenic pressures and climate have and will continue to accelerate stream bank and bed deposition but also other types of erosion. A framework with a cadre of different methodologies to monitor and understand erosion is a necessity, especially in climate change-vulnerable regions such as the Mediterranean. This is what this study tried to achieve by showcasing different methods that can be used at different scales and with different accuracy. In addition, all of these methods could be used together since they are complimentary to one another. Remote sensing products such as free satellite imagery and Google images can be the first step in order to identify stream bank changes over short periods of time (e.g., after a flood event) or over many years. UAVs can be utilized as a second step to provide higher accuracy and analysis at a larger scale (reach scale) of specific locations. Field measurements at the plot scale, such as erosion pins and cross-sections, can be used at a very narrow scale (specific bank), focusing on intense rainfall events or anthropogenic alterations (excavations) that change stream bed and bank morphology and provide validation data for the satellite and UAV images. Finally, through 3D terrestrial scanning, the determination of accelerated bank erosion or deposition is more accurate and enables the land managers to identify vulnerable areas to erosion and deposition. Once these areas are identified, nature-based solution should be implemented by land managers in order to stabilize stream banks, reduce erosion or deposition rates and consequently mitigate non-point source pollutants. Nature-based solutions are preferred because they try to emulate nature, thus reducing the acceleration of erosion and deposition. This proposed framework has high utility since it will allow managers to target the areas that produce the greatest erosion and deposition, and thus utilize funds more cost-effectively and promote sustainable management. In addition, because of the better erosion mitigating results, this framework is more likely to achieve the approval of the policy makers and general public, thus helping obtain the needed funding.

Author Contributions: Conceptualization, G.N.Z.; methodology, G.N.Z., P.K. and M.X.; software, P.K., G.G. and G.P.; validation, G.N.Z., V.I. and I.K.; analysis P.K., G.N.Z., G.G., M.X. and G.P.; data curation, P.K., G.G., G.P., I.K., M.X., A.S., K.K. and T.K.; writing—original draft preparation, P.K., G.G. and I.K.; writing—review and editing, P.K., G.N.Z. and V.I.; visualization, P.K., G.G. and G.P.; supervision, G.N.Z.; project administration, G.N.Z. All authors have read and agreed to the published version of the manuscript.

Data Availability Statement: Data and reports are available at http://websites3.teiemt.gr/p4sea. (accessed on 30 December 2023).

Conflicts of Interest: The authors declare no conflict of interest. The funders had no role in the design of the study; in the collection, analyses or interpretation of data; in the writing of the manuscript; or in the decision to publish the results.

References

1. Pimentel, D. Soil erosion: A food and environmental threat. *Environ. Dev. Sustain.* **2006**, *8*, 119–137. [CrossRef]
2. Zaimes, G.N.; Schultz, R.C. Riparian land-use impacts on bank erosion and deposition of an incised stream in north-central Iowa, USA. *Catena* **2015**, *125*, 61–73. [CrossRef]
3. Zaimes, G.N.; Tamparopoulos, A.E.; Tufekcioglu, M.; Schultz, R.C. Understanding stream bank erosion and deposition in Iowa, USA: A seven-year study along streams in different regions with different riparian land-uses. *J. Environ. Manag.* **2021**, *287*, 112352. [CrossRef]
4. Zaimes, G.N. Mediterranean riparian areas–climate change implications and recommendations. *J. Environ. Biol.* **2020**, *41*, 957–965. [CrossRef]
5. Simon, A.; Rinaldi, M. Disturbance, stream incision, and channel evolution: The roles of excess transport capacity and boundary materials in controlling channel response. *Geomorphology* **2006**, *79*, 361–383. [CrossRef]
6. Schumm, S.A.; Holdbrook, J. Geomorphic and sedimentary response of rivers to tectonic deformation: A brief review and critique of a tool for recognizing subtle epeirogenic deformation in modern and ancient settings. *Tectonophysics* **1999**, *305*, 287–306.
7. Bull, W.B. Discontinuous ephemeral streams. *Geomorphology* **1997**, *19*, 227–276. [CrossRef]
8. Pollen-Bankhead, N.; Simon, A. Hydrologic and hydraulic effects of riparian root networks on streambank stability: Is mechanical root-reinforcement the whole story? *Geomorphology* **2010**, *116*, 353–362. [CrossRef]
9. Wynn, T.M.; Henderson, M.B.; Vaughan, D.H. Changes in streambank erodibility and critical shear stress due to subaerial processes along a headwater stream, southwestern Virginia, USA. *Geomorphology* **2008**, *97*, 260–273. [CrossRef]
10. Langendoen, E.J.; Richard Lowrance, R.; Simon, A. Assessing the impact of riparian processes on streambank stability. *Ecohydrol. Ecosyst. Land Water Process Interact. Ecohydrol.* **2009**, *2*, 360–369. [CrossRef]
11. Koutalakis, P.; Zaimes, G.N.; Iakovoglou, V.; Ioannou, K. Reviewing soil erosion in Greece. *Int. J. Geol. Geotech. Eng.* **2015**, *9*, 936–941.
12. Zaimes, G.N.; Tufekcioglu, M.; Schultz, R.C. Riparian land-use impacts on stream bank and gully erosion in agricultural watersheds: What we have learned. *Water* **2019**, *11*, 1343. [CrossRef]
13. Zaimes, G.N. Utilizing new and innovative tools to mitigate surficial erosion in Mediterranean environments. *Kastamonu Univ. Orman Fak. Derg.* **2017**, *17*, 373–382. [CrossRef]
14. Lawler, D.M. The importance of high-resolution monitoring in erosion and deposition dynamics studies: Examples from estuarine and fluvial systems. *Geomorphology* **2005**, *64*, 1–23. [CrossRef]
15. Resop, J.P.; Hession, W.C. Terrestrial Laser Scanning for Monitoring Streambank Retreat: Comparison with Traditional Surveying Techniques. *J. Hydraul. Eng.* **2010**, *136*, 794–798. [CrossRef]
16. McBride, M. Riparian Reforestation and Channel Morphology. Ph.D. Dissertation, University of Vermont, Burlington, VT, USA, 2007.
17. King, C.; Baghdadi, N.; Lecomte, V.; Cerdan, O. The application of remote-sensing data to monitoring and modelling of soil erosion. *Catena* **2005**, *62*, 79–93. [CrossRef]
18. Benzer, N. Using the geographical information system and remote sensing techniques for soil erosion assessment. *Pol. J. Environ. Stud.* **2010**, *19*, 881–886.
19. Ganasri, B.P.; Ramesh, H. Assessment of soil erosion by RUSLE model using remote sensing and GIS-A case study of Nethravathi Basin. *Geosci. Front.* **2016**, *7*, 953–961. [CrossRef]
20. Shen, Z.Y.; Gong, Y.W.; Li, Y.H.; Hong, Q.; Xu, L.; Liu, R.M. A comparison of WEPP and SWAT for modeling soil erosion of the Zhangjiachong Watershed in the Three Gorges Reservoir Area. *Agric. Water Manag.* **2009**, *96*, 1435–1442. [CrossRef]
21. Szabó, S.; Gácsi, Z.; Balázs, B. Specific features of NDVI, NDWI and MNDWI as reflected in land cover categories. *Acta Geogr. Debr. Landsc. Environ. Ser.* **2016**, *10*, 194–202. [CrossRef]
22. Kosmas, C.; Danalatos, N.; Cammeraat, L.H.; Chabart, M.; Diamantopoulos, J.; Farand, R.; Gutierrez, L.; Jacob, A.; Marques, H.; Martinez-Fernandez, J.; et al. The effect of land use on runoff and soil erosion rates under Mediterranean conditions. *Catena* **1997**, *29*, 45–59. [CrossRef]
23. Koutalakis, P.; Tzoraki, O.; Gkiatas, G.; Zaimes, G.N. Using UAV to capture and record torrent bed and banks, flood debris, and riparian areas. *Drones* **2020**, *4*, 77. [CrossRef]
24. Eisenbeiss, H. UAV photogrammetry in plant science and geology, In Proceedings of the 6th ARIDA Workshop on "Innovations in 3D Measurement, Modelling and Visualization", Trento, Italy, 25–26 February 2008.
25. Wallace, L.; Lucieer, A.; Watson, C.; Turner, D. Development of a UAV-LiDAR system with application to forest inventory. *Remote Sens.* **2012**, *4*, 1519–1543. [CrossRef]
26. Eisenbeiss, H.; Sauerbier, M. Investigation of UAV systems and flight modes for photogrammetric applications. *Photogramm. Rec.* **2011**, *26*, 400–421. [CrossRef]
27. Eker, R.; Alkan, E.; Aydin, A. A Comparative Analysis of UAV-RTK and UAV-PPK Methods in Mapping Different Surface Types. *Eur. J. For. Eng.* **2020**, *7*, 12–25. [CrossRef]

28. Taddia, Y.; Stecchi, F.; Pellegrinelli, A. Coastal mapping using DJI Phantom 4 RTK in post-processing kinematic mode. *Drones* **2020**, *4*, 9. [CrossRef]

29. Gabara, G.; Sawicki, P. Multi-variant accuracy evaluation of uav imaging surveys: A case study on investment area. *Sensors* **2019**, *19*, 5229. [CrossRef] [PubMed]

30. Ebrahim, M.A.B. 3D laser scanners' techniques overview. *Int. J. Sci. Res.* **2015**, *4*, 323–331.

31. Tong, X.; Liu, X.; Chen, P.; Liu, S.; Luan, K.; Li, L.; Liu, S.; Liu, X.; Xie, H.; Jin, Y.; et al. Integration of UAV-based photogrammetry and terrestrial laser scanning for the three-dimensional mapping and monitoring of open-pit mine areas. *Remote Sens.* **2015**, *7*, 6635–6662. [CrossRef]

32. Fröhlich, C.; Mettenleiter, M. Terrestrial laser scanning–new perspectives in 3D surveying. *Int. Arch. Photogramm. Remote Sens.* **2004**, *36*, W2.

33. Baltsavias, E.P. A comparison between photogrammetry and laser scanning. *ISPRS J. Photogramm. Remote Sens.* **1999**, *54*, 83–94. [CrossRef]

34. Wu, C.; Yuan, Y.; Tang, Y.; Tian, B. Application of terrestrial laser scanning (TLS) in the architecture, engineering and construction (AEC) industry. *Sensors* **2021**, *22*, 265. [CrossRef] [PubMed]

35. Telling, J.; Lyda, A.; Hartzell, P.; Glennie, C. Review of Earth science research using terrestrial laser scanning. *Earth Sci. Res.* **2017**, *169*, 35–68. [CrossRef]

36. Brasington, J.; Vericat, D.; Rychkov, I. Modeling river bed morphology, roughness, and surface sedimentology using high resolution terrestrial laser scanning. *Water Resour. Res.* **2012**, *48*, 11519. [CrossRef]

37. Heritage, G.L.; Milan, D.J. Terrestrial laser scanning of grain roughness in a gravel-bed river. *Geomorphology* **2009**, *113*, 4–11. [CrossRef]

38. Picco, L.; Mao, L.; Cavalli, M.; Buzzi, E.; Rainato, R.; Lenzi, M.A. Evaluating short-term morphological changes in a gravel-bed braided river using terrestrial laser scanner. *Geomorphology* **2013**, *201*, 323–334. [CrossRef]

39. Myers, D.T.; Rediske, R.R.; McNair, J.N. Measuring streambank erosion: A comparison of erosion pins, total station, and terrestrial laser scanner. *Water* **2019**, *11*, 1846. [CrossRef]

40. Longoni, L.; Papini, M.; Brambilla, D.; Barazzetti, L.; Roncoroni, F.; Scaioni, M.; Ivanov, V.I. Monitoring riverbank erosion in mountain catchments using terrestrial laser scanning. *Remote Sens.* **2016**, *8*, 241. [CrossRef]

41. Riegels, N.; Jensen, R.; Bensasson, L.; Banou, S.; Møller, F.; Bauer-Gottwein, P. Estimating resource costs of compliance with EU WFD ecological status requirements at the river basin scale. *J. Hydrol.* **2011**, *396*, 197–214. [CrossRef]

42. Pennos, C.; Lauritzen, S.E.; Pechlivanidou, S.; Sotiriadis, Y. Geomorphic constrains on the evolution of the Aggitis River Basin Northern Greece (a preliminary report). *Bull. Geol. Soc. Greece* **2016**, *50*, 365–373. [CrossRef]

43. Savopoulou, A.; Giatas, G.; Pagonis, G.; Iakovoglou, V.; Zaimes, G.N. Visual protocols and GIS as preliminary investigative tools to locate potential ecoengineering in streams and riparian areas. *Procedia Environ. Sci. Eng.* **2017**, *4*, 227–234.

44. Koutalakis, P.; Zaimes, G.; Ioannou, K.; Iakovoglou, V. Application of the SWAT model on torrents of the Menoikio, Greece. *Fresen. Environ. Bull.* **2017**, *26*, 1210–1215.

45. Segarra, J.; Buchaillot, M.L.; Araus, J.L.; Kefauver, S.C. Remote Sensing for Precision Agriculture: Sentinel-2 Improved Features and Applications. *J. Agron.* **2020**, *10*, 641. [CrossRef]

46. Szantoi, Z.; Strobl, P. Copernicus Sentinel-2 calibration and validation. *Eur. J. Remote Sens.* **2019**, *52*, 253–255. [CrossRef]

47. Li, J.; Roy, D.P. A global analysis of Sentinel-2A, Sentinel-2B and Landsat-8 data revisit intervals and implications for terrestrial monitoring. *Remote Sens.* **2017**, *9*, 902. [CrossRef]

48. Drusch, M.; Del Bello, U.; Carlier, S.; Colin, O.; Fernandez, V.; Gascon, F.; Bargellini, P. Sentinel-2: ESA's optical high-resolution mission for GMES operational services. *Remote Sens. Environ.* **2012**, *120*, 25–36. [CrossRef]

49. Chatziantoniou, A.; Petropoulos, G.P.; Psomiadis, E. Co-Orbital Sentinel 1 and 2 for LULC mapping with emphasis on wetlands in a mediterranean setting based on machine learning. *Remote Sens.* **2017**, *9*, 1259. [CrossRef]

50. Eid, A.N.M.; Olatubara, C.O.; Ewemoje, T.A.; Farouk, H.; El-Hennawy, M.T. Coastal wetland vegetation features and digital Change Detection Mapping based on remotely sensed imagery: El-Burullus Lake, Egypt. *Int. Soil Water Conserv. Res.* **2020**, *8*, 66–79.

51. Kashyap, M.; Bhatt, C.M.; Rawat, J.S. Application of Sentinel-2 Data for Extraction of Flood Inundation along Ganga River, Bihar. *Int. J. Mech. Eng. Res.* **2021**, *6*, 47–52. [CrossRef]

52. Bhandari, A.K.; Kumar, A.; Singh, G.K. Feature extraction using Normalized Difference Vegetation Index (NDVI): A case study of Jabalpur city. *Proc. Technol.* **2012**, *6*, 612–621. [CrossRef]

53. Johansen, B.; Tømmervik, H. The relationship between phytomass, NDVI and vegetation communities on Svalbard. *Int. J. Appl. Earth Obs. Geoinf.* **2014**, *27*, 20–30. [CrossRef]

54. Price, J.C.; Bausch, W.C. Leaf area index estimation from visible and near-infrared reflectance data. *Remote Sens. Environ.* **1995**, *52*, 55–65. [CrossRef]

55. Wang, J.; Rich, P.M.; Price, K.P.; Kettle, W.D. Relations between NDVI and tree productivity in the central Great Plains. *Int. J. Remote Sens.* **2004**, *25*, 3127–3138. [CrossRef]

56. Nanzad, L.; Zhang, J.; Tuvdendorj, B.; Nabil, M.; Zhang, S.; Bai, Y. NDVI anomaly for drought monitoring and its correlation with climate factors over Mongolia from 2000 to 2016. *J. Arid Environ.* **2019**, *164*, 69–77. [CrossRef]

57. Peters, A.J.; Walter-Shea, E.A.; Ji, L.; Vina, A.; Hayes, M.; Svoboda, M.D. Drought monitoring with NDVI-based standardized vegetation index. *Photogramm. Eng. Remote Sens.* **2002**, *68*, 71–75.

58. Gao, B.C. NDWI—A normalized difference water index for remote sensing of vegetation liquid water from space. *Remote Sens. Environ.* **1996**, *58*, 257–266. [CrossRef]

59. Bannari, A.; Guedon, A.M.; El-Ghmari, A. Mapping Slight and Moderate Saline Soils in Irrigated Agricultural Land Using Advanced Land Imager Sensor (EO-1) Data and Semi-Empirical Models. *Commun. Soil Sci. Plant Anal.* **2016**, *47*, 1883–1906. [CrossRef]

60. Aslam, B.; Maqsoom, A.; Salah Alaloul, W.; Musarat, M.A.; Jabbar, T.; Zafar, A. Soil erosion susceptibility mapping using a GIS-based multi-criteria decision approach: Case of district Chitral, Pakistan. *Ain Shams Eng. J.* **2021**, *12*, 1637–1649. [CrossRef]

61. Rose, C.W.; Williams, J.R.; Sander, G.C.; Barry, D.A. A mathematical model of soil erosion and deposition processes: I. Theory for a plane land element. *Soil Sci. Soc. Am. J.* **1983**, *47*, 991–995. [CrossRef]

62. Gómez-Gutiérrez, Á.; Conoscenti, C.; Angileri, S.E.; Rotigliano, E.; Schnabel, S. Using topographical attributes to evaluate gully erosion proneness (susceptibility) in two mediterranean basins: Advantages and limitations. *Nat. Hazards* **2015**, *79*, 291–314. [CrossRef]

63. McFeeters, S.K. The use of the Normalized Difference Water Index (NDWI) in the delineation of open water features. *Int. J. Remote Sens.* **1996**, *17*, 1425–1432. [CrossRef]

64. Chen, L.; Lety, H.; Fan, M.; Shang, H.; Tao, J.; Wu, L.; Zhang, Y.; Yu, C.; Gu, J.; Zhang, N.; et al. An Introduction to the Chinese High-Resolution Earth Observation System: Gaofen-1~7 Civilian Satellites. *J. Remote Sens.* **2022**, *2022*, 9769536. [CrossRef]

65. Coffer, M.M.; Schaeffer, B.A.; Darling, J.A.; Urquhart, E.A.; Salls, W.B. Quantifying national and regional cyanobacterial occurrence in US lakes using satellite remote sensing. *Ecol. Indic.* **2020**, *111*, 105976. [CrossRef]

66. Michez, A.; Philippe, L.; David, K.; Sébastien, C.; Christian, D.; Bindelle, J. Can low-cost unmanned aerial systems describe the forage quality heterogeneity? Insight from a Timothy Pasture case study in Southern Belgium. *Remote Sens.* **2020**, *12*, 1650. [CrossRef]

67. Manfreda, S.; Dal Sasso, S.F.; Pizarro, A.; Tauro, F. New insights offered by UAS for river monitoring. In *Applications of Small Unmanned Aircraft Systems: Best Practices and Case Studies*; Sharma, J.B., Ed.; CRC Press, Taylor and Francis Group: New York, NY, USA, 2019; pp. 211–234.

68. Hung, I.; Unger, D.; Kulhavy, D.; Zhang, Y. Positional precision analysis of orthomosaics derived from drone captured aerial imagery. *Drones* **2019**, *3*, 46. [CrossRef]

69. Psirofonia, P.; Samaritakis, V.; Eliopoulos, P.; Potamitis, I. Use of unmanned aerial vehicles for agricultural applications with emphasis on crop protection: Three novel case-studies. *J. Agric. Sci. Technol.* **2017**, *5*, 30–39. [CrossRef]

70. Ihsan, M.; Somantri, L.; Sugito, N.T.; Himayah, S.; Affriani, A.R. The Comparison of Stage and Result Processing of Photogrammetric Data Based on Online Cloud Processing. In Proceedings of the IGEOS International Geography Seminar, IOP Conference Series: Earth and Environmental Science, Tanjong Malim, Malaysia, 3–4 December 2018.

71. Firdaus, M.I.; Rau, J.Y. Comparisons of the three-dimensional model reconstructed using MicMac, PIX4D mapper and Photoscan Pro. In Proceedings of the 38th Asian Conference on Remote Sensing-Space Applications: Touching Human Lives 2017, New Delhi, India, 23–27 October 2017.

72. Jugie, M.; Gob, F.; Virmoux, C.; Brunstein, D.; Tamisier, V.; Le Coeur, C.; Grancher, D. Characterizing and quantifying the discontinuous bank erosion of a small low energy river using Structure-from-Motion Photogrammetry and erosion pins. *J. Hydrol.* **2018**, *563*, 418–434. [CrossRef]

73. Simon, A.; Curini, A.; Darby, S.; Langendoen, E. Streambank mechanics and the role of bank and near-bank processes in incised channels. In *Incised River Channels*; Darby, S., Simon, A., Eds.; John Wiley: London, UK, 1999; pp. 123–152.

74. Hooke, J.M. Magnitude and distribution of rates of riverbank erosion. *Earth Surf. Process Landf.* **1979**, *5*, 143–157. [CrossRef]

75. Gkiatas, G.T.; Koutalakis, P.D.; Kasapidis, I.K.; Iakovoglou, V.; Zaimes, G.N. Monitoring and Quantifying the Fluvio-Geomorphological Changes in a Torrent Channel Using Images from Unmanned Aerial Vehicles. *Hydrology* **2022**, *9*, 184. [CrossRef]

76. Lopac, N.; Jurdana, E.; Brnelic, A.; Krljan, T. Application of Laser Systems for Detection and Ranging in the Modern Road Transportation and Maritime Sector. *Sensors* **2022**, *22*, 5946. [CrossRef]

77. Liang, X.; Kankare, V.; Hyyppä, J.; Wang, Y.; Kukko, A.; Haggrén, H.; Yu, X.; Kaartinen, H.; Jaakkola, A.; Guan, F.; et al. Terrestrial laser scanning in forest inventories. *ISPRS J. Photogramm. Remote Sens.* **2016**, *115*, 63–77. [CrossRef]

78. Wenzel, K.; Rothermel, M.; Fritsch, D.; Haala, N. Image acquisition and model selection for multi-view stereo. *Int. Arch. Photogramm. Remote Sens. Spat. Inf. Sci.* **2013**, *40*, 251–258. [CrossRef]

79. Diaconu, D.C.; Koutalakis, P.D.; Gkiatas, G.T.; Dascalu, G.V.; Zaimes, G.N. River Sand and Gravel Mining Monitoring Using Remote Sensing and UAVs. *Sustainability* **2023**, *15*, 1944. [CrossRef]

80. Zhao, Q.; Yu, L.; Du, Z.; Peng, D.; Hao, P.; Zhang, Y.; Gong, P. An overview of the applications of earth observation satellite data: Impacts and future trends. *Remote Sens.* **2022**, *14*, 1863. [CrossRef]

81. Ouma, Y.O. Advancements in medium and high resolution Earth observation for land-surface imaging: Evolutions, future trends and contributions to sustainable development. *Adv. Space Res.* **2016**, *57*, 110–126. [CrossRef]

82. Smith, M.J.; Pain, C.F. Applications of remote sensing in geomorphology. *Prog. Phys. Geogr.* **2009**, *33*, 568–582. [CrossRef]

83. Boothroyd, R.J.; Williams, R.D.; Hoey, T.B.; Barrett, B.; Prasojo, O.A. Applications of Google Earth Engine in fluvial geomorphology for detecting river channel change. *Wiley Interdiscip. Rev. Water* **2021**, *8*, e21496. [CrossRef]

84. Ablat, X.; Liu, G.; Liu, Q.; Huang, C. Using MODIS-NDVI time series to quantify the vegetation responses to river hydro-geomorphology in the wandering river floodplain in an arid region. *Water* **2021**, *13*, 2269. [CrossRef]

85. Ouyang, W.; Hao, F.; Skidmore, A.K.; Toxopeus, A.G. Soil erosion and sediment yield and their relationships with vegetation cover in upper stream of the Yellow River. *Sci. Total Environ.* **2010**, *409*, 396–403. [CrossRef] [PubMed]

86. Williams, F.; Moore, P.; Isenhart, T.; Tomer, M. Automated measurement of eroding streambank volume from high-resolution aerial imagery and terrain analysis. *Geomorphology* **2020**, *367*, 107313. [CrossRef]

87. Bannari, A.; Kadhem, G.; El-Battay, A.; Hameid, N.A.; Rouai, M. Assessment of land erosion and sediment accumulation caused by runoff after a flash-flooding storm using topographic profiles and spectral indices. *Adv. Remote Sens.* **2016**, *5*, 315–354. [CrossRef]

88. Tha, T.; Piman, T.; Bhatpuria, D.; Ruangrassamee, P. Assessment of riverbank erosion hotspots along the mekong river in cambodia using remote sensing and hazard exposure mapping. *Water* **2022**, *14*, 1981. [CrossRef]

89. Xu, H. Modification of normalised difference water index (NDWI) to enhance open water features in remotely sensed imagery. *Int. J. Remote Sens.* **2006**, *27*, 3025–3033. [CrossRef]

90. Laonamsai, J.; Julphunthong, P.; Saprathet, T.; Kimmany, B.; Ganchanasuragit, T.; Chomcheawchan, P.; Tomun, N. Utilizing NDWI, MNDWI, SAVI, WRI, and AWEI for Estimating Erosion and Deposition in Ping River in Thailand. *Hydrology* **2023**, *10*, 70. [CrossRef]

91. Benda, L.E.E.; Poff, N.L.; Miller, D.; Dunne, T.; Reeves, G.; Pess, G.; Pollock, M. The network dynamics hypothesis: How channel networks structure riverine habitats. *BioScience* **2004**, *54*, 413–427. [CrossRef]

92. Vrieling, A. *Mapping Erosion from Space*; Wageningen University and Research: Wageningen, The Netherlands, 2007.

93. Desprats, J.F.; Raclot, D.; Rousseau, M.; Cerdan, O.; Garcin, M.L.; Le Bissonnais, Y.; Ben Slimane, A.; Fouché, J.; Monfort-Climent, D. Mapping linear erosion features using high and very high resolution satellite imagery. *Land Degrad. Dev.* **2013**, *24*, 22–32. [CrossRef]

94. Vrieling, A.; de Jong, S.M.; Sterk, G.; Rodrigues, S.C. Timing of erosion and satellite data: A multi-resolution approach to soil erosion risk mapping. *Int. J. Appl. Earth Obs. Geoinf.* **2008**, *10*, 267–281. [CrossRef]

95. Saadat, H.; Adamowski, J.; Tayefi, V.; Namdar, M.; Sharifi, F.; Ale-Ebrahim, S. A new approach for regional scale interrill and rill erosion intensity mapping using brightness index assessments from medium resolution satellite images. *Catena* **2014**, *113*, 306–313. [CrossRef]

96. Phinzi, K.; Holb, I.; Szabó, S. Mapping permanent gullies in an agricultural area using satellite images: Efficacy of machine learning algorithms. *Agronomy* **2021**, *11*, 333. [CrossRef]

97. Hamada, Y.; O'Connor, B.L.; Orr, A.B.; Wuthrich, K.K. Mapping ephemeral stream networks in desert environments using very-high-spatial-resolution multispectral remote sensing. *J. Arid. Environ.* **2016**, *130*, 40–48. [CrossRef]

98. Liu, G.; Zheng, F.; Wilson, G.V.; Xu, X.; Liu, C. Three decades of ephemeral gully erosion studies. *Soil Tillage Res.* **2021**, *212*, 105046. [CrossRef]

99. Fiorucci, F.; Ardizzone, F.; Rossi, M.; Torri, D. The use of stereoscopic satellite images to map rills and ephemeral gullies. *Remote Sens.* **2015**, *7*, 14151–14178. [CrossRef]

100. Jacobsen, K. Which Satellite Image should be used for Mapping. *ISPRS Ann. Photogramm. Remote Sens. Spat. Inf. Sci.* **2023**, *10*, 827–834. [CrossRef]

101. Petitjean, F.; Inglada, J.; Gancarski, P. Assessing the quality of temporal high-resolution classifications with low-resolution satellite image time series. *Int. J. Remote Sens.* **2014**, *35*, 2693–2712. [CrossRef]

102. Stroosnijder, L. Measurement of erosion: Is it possible? *Catena* **2005**, *64*, 162–173. [CrossRef]

103. Tmušić, G.; Manfreda, S.; Aasen, H.; James, M.R.; Gonçalves, G.; Ben-Dor, E.; Brook, A.; Polinova, M.; Arranz, J.J.; János Mészáros, K.; et al. Current practices in UAS-based environmental monitoring. *Remote Sens.* **2020**, *12*, 1001. [CrossRef]

104. McCabe, M.F.; Rodell, M.; Alsdorf, D.E.; Miralles, D.G.; Uijlenhoet, R.; Wagner, W.; Lucieer, A.; Houborg, R.; Verhoest, N.E.C.; Franz, T.E.; et al. The future of Earth observation in hydrology. *Hydrol. Earth Syst. Sci.* **2017**, *21*, 3879–3914. [CrossRef]

105. Meinen, B.U.; Robinson, D.T. Streambank topography: An accuracy assessment of UAV-based and traditional 3D reconstructions. *Int. J. Remote Sens.* **2020**, *41*, 1–18. [CrossRef]

106. García-Ruiz, J.M.; Nadal-Romero, E.; Lana-Renault, N.; Beguería, S. Erosion in Mediterranean landscapes: Changes and future challenges. *Geomorphology* **2013**, *198*, 20–36. [CrossRef]

107. Zaimes, G.N.; Schultz, R.C.; Isenhart, T.M. Stream bank erosion adjacent to riparian forest buffers, row-crop fields, and continuously-grazed pastures along Bear Creek in central Iowa. *J. Soil Water Conserv.* **2004**, *59*, 19–27.

108. Reichenbach, P.; Busca, C.; Mondini, A.C.; Rossi, M. The Influence of Land Use Change on Landslide Susceptibility Zonation: The Briga Catchment Test Site (Messina, Italy). *Environ. Manag.* **2014**, *54*, 1372–1384. [CrossRef]

109. Heede, B.H. Deteriorated watersheds can be restored: A case study. *J. Environ. Manag.* **1979**, *3*, 271–281. [CrossRef]

110. Knevels, R.; Brenning, A.; Gingrich, S.; Heiss, G.; Lechner, T.; Leopold, P.; Plutzar, C.; Proske, H.; Petschko, H. Towards the use of land use legacies in landslide modeling: Current challenges and future perspectives in an austrian case study. *Land* **2021**, *10*, 954. [CrossRef]

111. Tsanis, I.K.; Seiradakis, K.D.; Sarchani, S.; Panagea, I.S.; Alexakis, D.D.; Koutroulis, A.G. The Impact of Soil-Improving Cropping Practices on Erosion Rates: A Stakeholder-Oriented Field Experiment Assessment. *Land* **2021**, *10*, 964. [CrossRef]
112. Fan, L.; Powrie, W.; Smethurst, J.; Atkinson, P.M.; Einstein, H. The effect of short ground vegetation on terrestrial laser scans at a local scale. *ISPRS J. Photogramm. Remote Sens.* **2014**, *95*, 42–52. [CrossRef]
113. Vázquez-Tarrío, D.; Ruiz-Villanueva, V.; Garrote, L.; Benito, G.; Calle, M.; Lucía, A.; Díez-Herrero, A. Effects of sediment transport on flood hazards: Lessons learned and remaining challenges. *Geomorphology* **2024**, *446*, 108976. [CrossRef]
114. Petalas, C.P.; Moutsopoulos, K.N. Hydrogeologic behavior of a complex and mature karst aquifer system under drought condition. *Environ. Process* **2019**, *6*, 643–671. [CrossRef]
115. Guan, M.; Wright, N.G.; Sleigh, P.A. Multiple effects of sediment transport and geomorphic processes within flood events: Modelling and understanding. *Int. J. Sediment Res.* **2015**, *30*, 371–381. [CrossRef]
116. Owens, P.N. Soil erosion and sediment dynamics in the Anthropocene: A review of human impacts during a period of rapid global environmental change. *J. Soils Sediments* **2020**, *20*, 4115–4143. [CrossRef]
117. Lespez, L. Geomorphic responses to long-term land use changes in Eastern Macedonia (Greece). *Catena* **2003**, *51*, 181–208. [CrossRef]
118. Walsh, K.; Berger, J.F.; Roberts, C.N.; Vanniere, B.; Ghilardi, M.; Brown, A.G.; Woodbridge, J.; Lespez, L.; Estrany, J.; Glais, A.; et al. Holocene demographic fluctuations, climate and erosion in the Mediterranean: A meta data-analysis. *Holocene* **2019**, *29*, 864–885. [CrossRef]
119. Woodget, A.S.; Austrums, R.; Maddock, I.P.; Habit, E. Drones and digital photogrammetry: From classifications to continuums for monitoring river habitat and hydromorphology. *Wiley Interdiscip. Rev. Water* **2017**, *4*, e1222. [CrossRef]